

Article

A Combined EMPA and LA-ICP-MS Study of Muscovite from Pegmatites in the Chinese Altai, NW China: Implications for Tracing Rare-Element Mineralization Type and Ore-Forming Process

Qifeng Zhou ^{1,*}, Kezhang Qin ^{2,3,4,*}, Dongmei Tang ^{2,3} and Chunlong Wang ⁵

- ¹ Institute of Mineral Resources Research, China Metallurgical Geology Bureau, Beijing 101300, China
² Key Laboratory of Mineral Resources, Institute of Geology and Geophysics, Chinese Academy of Sciences, Beijing 100029, China; tdm@mail.igcas.ac.cn
³ Institutions of Earth Sciences, Chinese Academy of Sciences, Beijing 100029, China
⁴ College of Earth and Planetary Sciences, University of Chinese Academy of Sciences, Beijing 100049, China
⁵ State Key Laboratory of Geological Process and Mineral Resources, Key Laboratory of Geological Survey and Evaluation of Ministry of Education, School of Earth Resources, China University of Geosciences, Wuhan 430074, China; chunlong-wang@hotmail.com
* Correspondence: zhouqifeng85@163.com (Q.Z.); kzq@mail.igcas.ac.cn (K.Q.)



Citation: Zhou, Q.; Qin, K.; Tang, D.; Wang, C. A Combined EMPA and LA-ICP-MS Study of Muscovite from Pegmatites in the Chinese Altai, NW China: Implications for Tracing Rare-Element Mineralization Type and Ore-Forming Process. *Minerals* **2022**, *12*, 377. <https://doi.org/10.3390/min12030377>

Academic Editors: Jiankang Li, Peng Li and Harald G. Dill

Received: 16 February 2022

Accepted: 15 March 2022

Published: 18 March 2022

Publisher's Note: MDPI stays neutral with regard to jurisdictional claims in published maps and institutional affiliations.



Copyright: © 2022 by the authors. Licensee MDPI, Basel, Switzerland. This article is an open access article distributed under the terms and conditions of the Creative Commons Attribution (CC BY) license (<https://creativecommons.org/licenses/by/4.0/>).

Abstract: The mineralogical studies of rare-element (REL) pegmatites are important for unraveling the ore-forming process and evaluating REL mineralization potential. The Chinese Altai orogenic belt hosting more than 100,000 pegmatite dykes is famous for rare-metal resources worldwide and diverse REL mineralization types. In this paper, we present the results of EMPA and LA-ICP-MS for muscovite from the typical REL pegmatite dykes of the Chinese Altai. The studied pegmatites are Li-Be-Nb-Ta, Li-Nb-Ta, Nb-Ta, Be-Nb-Ta, Be and barren pegmatites. The Li⁺ accompanied with Fe, Mg and Mn substitute for Al³⁺ at the octahedral site in muscovite from the REL pegmatites, and the substitution of Rb by Cs at the interlayer space is identified in muscovite from the Be pegmatites. The P and B contents increase with evolution degree and the lenses from the Nb-Ta pegmatite are produced at late fluid-rich stage with high fluxes (P and B). The enrichment of HFSE in muscovite indicates a Nb-Ta-Sn-W rich pegmatite magma for the Be-Nb-Ta pegmatite. From barren pegmatite, beryl-bearing zone, to spodumene-bearing zone, the evolution degrees of pegmatite-forming magmas progressively increase. In the Chinese Altai, the possible indicators of muscovite for REL mineralization types include Rb (ca. 400–600 ppm, barren pegmatite; ca. 1200–4000 ppm, Be pegmatite; >4500 ppm, Li pegmatite), Cs (ca. 5–50 ppm, barren pegmatite; ca. 100–500 ppm, Be pegmatite; >300 ppm, Li pegmatite) and Ge (<3 ppm, barren pegmatite; ca. 4–6 ppm, Be pegmatite; ca. 6–12 ppm, Li pegmatite) coupled with Ta, Be (both <10 ppm, barren pegmatite) and FeO (ca. 3–4 wt%, Be pegmatite; ca. 1–2.5 wt%, Li pegmatite). The plots of Nb/Ta vs. Cs and K/Rb vs. Ge are proposed to discriminate barren, Be- and Nb-Ta-(Li-Be-Rb-Cs) pegmatites. The Li, Be, Rb, Cs and F concentrations of forming liquid are evaluated based on the trace element compositions of muscovite. The high Rb and Cs contents of liquid and lower Be contents than beryl saturation value indicate that both highly evolved pegmatite magma and low temperature at emplacement contribute to beryl formation. The liquids saturated with spodumene have large variations of Li, possibly related to metastable state at Li unsaturation-supersaturation or heterogeneous distribution of lithium in the system.

Keywords: muscovite; pegmatite; LA-ICP-MS; degree of evolution; rare-element mineralization; Altai

1. Introduction

Granitic pegmatites hosting lots of rare elements (RELS) are the important targets for REL prospecting. The puzzles on genesis of granitic pegmatites and REL mineralization

have always been explored. Most granitic pegmatites are interpreted as products of granitic fractionation and evolution [1,2], in which process rare elements and fluxes accumulate in residual melt [3–5]. Corresponding to various subtypes of granitic pegmatites and diverse REL mineralization types, the evolution degrees of pegmatite magma are different [6–8]. It is important to show the characteristics of pegmatite magma enriched in REL, clarify the evolution degrees to estimate the potential of REL enrichment and compare the differences of different REL mineralization types to look for potential indicators.

Mica is one of the most common rock-forming minerals for pegmatite. Micas occurring in pegmatites include biotite, muscovite, zinnwaldite, poly lithionite, lepidolite, etc. The highly structural and chemical flexibility for micas make them become repositories for major, minor and trace elements that do not favorably enter into quartz and feldspars which are the major mineral phases [9,10]. The compositions of micas and changes among different mica types reflect the conditions of crystallization of magmas, including the evolution degree of melts [11–14] and the redox state [10], and further reveal the origins of magma [15–17]. Micas formed from higher evolved magma normally show enrichment in Li, Rb, Cs and F, with decrease in Mg, Ti and the K/Rb values, both from the external to internal zones in individual zoned bodies and from pegmatites with different degrees of evolution [7,12–14,18–26]. Muscovite as the most common mica during the whole pegmatite evolution and among diverse REL pegmatites is a good petrogenetic indicator of pegmatite evolution and REL mineralization. The incompatible trace element contents of the respective liquids (magma enriched in different REL) that are reconstructed from compositions of muscovite also show a correlation with REL mineralization types [27], supplying a way to survey REL-rich pegmatite magma.

The Chinese Altai orogenic belt, as the important part of the Central Asian Orogenic Belt, hosts more than 100,000 pegmatite dykes and a lot of REL resources. The REL mineralization types (Li-Be-Nb-Ta, Li-Nb-Ta, Nb-Ta, Be-Nb-Ta, Be and barren) of the REL pegmatites have been recognized [28]. These REL pegmatites with distinct features on internal zone patterns, mineralogy components, formation ages and country rocks are good examples to study the mineral indicators for REL mineralization and to reveal the REL enrichment. The previous studies mostly focus on formation ages and petrogenesis of the REL pegmatites [29–38], and concentrate on melt-fluid evolution and origin of the Koktokay No. 3 pegmatite, which is the largest Li-Be-Nb-Ta-Cs pegmatite deposit in the Chinese Altai [28,39–46]. This paper is concerned with muscovite from the typical pegmatites of diverse REL mineralization types in the Chinese Altai, since muscovite is the most common mica here. We present results of major and trace element compositions of muscovite. The chemical differences and compositional trends of muscovite would have been summarized to clarify the evolution degrees of the typical REL pegmatite dykes, and identify tracers that are proxies for various REL mineralization types. Moreover, some REL concentrations of pegmatite magmas are reconstructed to further reveal the Be and Li ore-forming process. This would shed light on REL mineralization mechanisms and be beneficial for rare-metal prospecting in this region to some extent.

2. Regional Geological Setting

The Altai orogenic belt is situated between the Sayan and Gorny Altai of southern Siberia to the north and the Junggar block to the south [47]. It comprises the Mongolian Altai, Chinese Altai and Russian Altai from east to west. The Chinese Altai, divided into six fault-bounded integral parts (the Altaishan terrane, the NW Altaishan terrane, the Central Altaishan terrane, the Qiongkuer-Abagong terrane, the Erqis terrane and the Perkin-Ertai terrane [48]), is composed of various deformed and metamorphosed Vendian to Paleozoic sedimentary, volcanic and granitic rocks [49–56]. The Chinese Altai is described as a middle Cambrian to early Permian magmatic arc [48,51–57]. It underwent a complex evolution of subduction and accretion events in the Paleozoic period [47,57–60], shown by ocean ridge subduction, massive granitic magma activities and Devonian high-temperature metamorphism [54,55,61], and completed the basic tectonic framework no later than the

middle the Carboniferous period [48,57,59,62,63]. Then, the Chinese Altai progressed into the development of a relatively stable continent with alternating moderate tension and compression events. During the convergence between the Chinese Altai and the East and West Junggar arcs in the Permian [64,65] and the amalgamation of the Siberia and Tarim cratons in the Triassic [66], the major REL pegmatites formed accompanied with relatively small granitic magma activities [33,52,67–70].

3. Geology of Pegmatites

The pegmatite dykes in the Chinese Altai mostly occur within the Central Altaishan terrane and the Qiongkuer-Abagong terrane (Figure 1). The pegmatite dykes in the Chinese Altai are divided into nine pegmatite fields (Qinghe, Keketuohai, Kuwei-Jiebiete, Kelumute-Jideke, Kalaeerqisi, Dakalasu-Kekexier, Xiaokalasu-Qiebielin, Hailiutan-Yeliuman and Jiamanhaba, Figure 1) [28] and grouped into three mineralization types, which are muscovite, muscovite rare element (muscovite-REL) and rare element (REL). The formation times of these three-type pegmatites are 476–426 Ma [31,34], 369 Ma [32] and 403–154 Ma [29,35–38,68,70–72], respectively. The REL pegmatites formed in 403–386 Ma, 333–253 Ma and 250–154 Ma [29,35–38,68,70–72], corresponding to the orogenic stages of the Chinese Altai, including syn-orogenic (420–360 Ma), late-orogenic (350–250 Ma) and post-orogenic (250–180 Ma) settings [38,50,53,54,73,74]. The REL pegmatites formed in syn-orogenic settings are scarce, and those formed in late to post-orogenic settings are the major REL prospecting targets in the Chinese Altai [37]. Some of the REL pegmatite dykes are Be, Be-Nb-Ta, Li-Nb-Ta, Li-Be-Nb-Ta and Li-Be-Nb-Ta-Rb-Cs deposits [28].

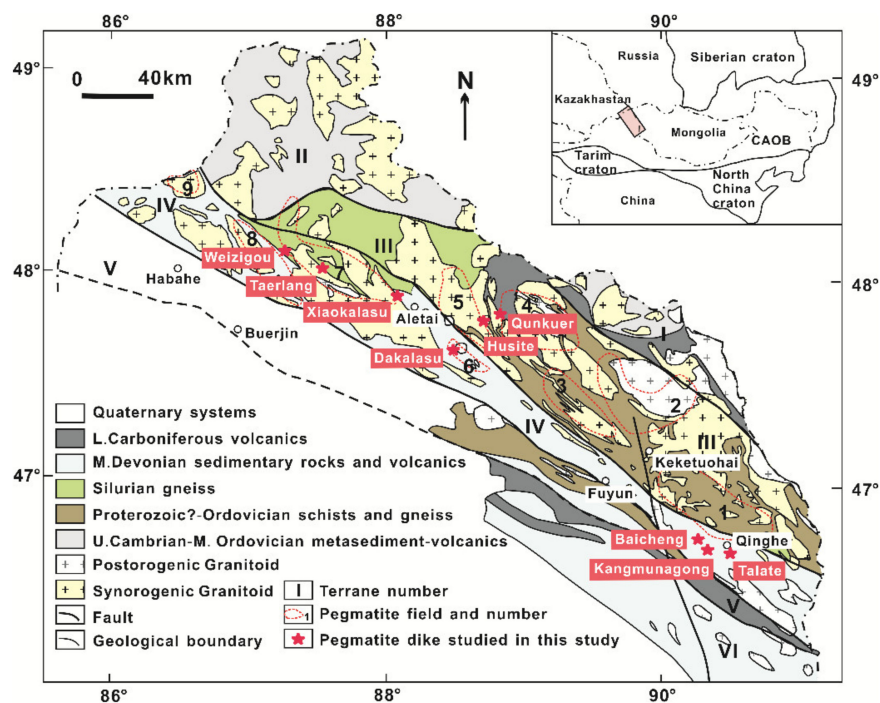


Figure 1. Geological sketch map of the Chinese Altai, modified from [47,49,57,72]. I, Altaishan terrane; II, NW Altaishan terrane; III, Central Altaishan terrane; IV, Qiongkuer-Abagong terrane; V, Erqis terrane; VI, Perkin-Ertai terrane. 1, Qinghe pegmatite field; 2, Keketuohai pegmatite field; 3, Kuwei-Jiebiete pegmatite field; 4, Kelumute-Jideke pegmatite field; 5, Kalaeerqisi pegmatite field; 6, Dakalasu-Kekexier pegmatite field; 7, Xiaokalasu-Qiebielin pegmatite field; 8, Hailiutan-Yeliuman pegmatite field; 9, Jiamanhaba pegmatite field.

In this study, seven typical REL pegmatite deposits and two barren pegmatite dykes from four pegmatite fields in the Chinese Altai are investigated (Figure 1). The Talate (Li-Be-Nb-Ta), Baicheng (Nb-Ta) and Kangmunagong (barren) pegmatite dykes are located in the Qinghe pegmatite field. The Qunkuer (Be) and Husite (Be) pegmatites belong to

Kelumute-Jideke pegmatite field. The Dakalasu (Be-Nb-Ta) pegmatite is typical in the Dakalasu-Kekexier pegmatite field. The Xiaokalasu (Li-Nb-Ta), Weizigou (Be) and Taerlang (Barren) belong to the Xiaokalasu-Qiebielin pegmatite fields. The types, internal zonation patterns, mineralogy components, formation ages and country rocks of these pegmatites are listed in Table 1. Compared with the barren pegmatites, the REL pegmatites show complex internal zones. There is no obvious correlation between REL-mineralization types and formation times [72]. The studied pegmatites mostly formed in the Permian to early Jurassic period [38,72]. The country rocks of the Dakalasu and Weizigou pegmatites are granites with large age discrepancies [75,76], and the rest of the studied pegmatites are mainly hosted in the middle Ordovician and middle Devonian mica schists (Figure 1) [53,77].

Table 1. Main characteristics of the pegmatite dykes studied in the Chinese Altai.

Pegmatite	Pegmatite Field	Pegmatite Type	Pegmatite Subtype	Mineralization Type	Internal Zonation and Mineralogy Components	Ages	Country Rock
Talate	Qinghe	complex	spodumene	Li-Be-Nb-Ta	WZ: fine Ab-Qz-Ms-Grt-Brl; OIZ: graphic intergrowth; IIZ: Spd-Qz-Ab; CZ: blocky Mc and Qz block.	286 Ma * [72], 386 Ma [37]	Mica schist
Baicheng	Qinghe	beryl	beryl-columbite	Nb-Ta	Kf-Ab-Qz-Ms; lenses: Mc block and Qz-Ms-CGM-Tur block; MU: saccharoidal Ab-Qz-Ms.	297 Ma * [72]	Mica schist
Kangmunagong	Qinghe			Barren	Homogeneous body: Kf-Ab-Qz-Ms-Tur-Grt.	265 Ma * [72]	Mica schist
Qunkuer	Kelumute-Jideke	beryl	beryl-columbite	Be	saccharoidal Ab-Qz-Ms; coarse Grt-Ab intergrowth; Mc block; smoky Qz-Brl-Ms	194 Ma [72]	Mica schist
Husite	Kelumute-Jideke	beryl	beryl-columbite	Be	BZ: fine Ab-Qz-Ms; WZ: coarse Ms-Qz-Brl-Grt; IZ: blocky Mc and graphic intergrowth with Brl; MU: saccharoidal Ab.	199 Ma [72]	Mica schist
Dakalsu	Dakalsu-Kekexier	beryl	beryl-columbite	Be-Nb-Ta	BZ: fine Ab-Qz-Ms-Grt-Tur; WZ: graphic intergrowth-CGM; IZ: Mc block-Qz-Ms-Brl columns-CGM; MU: Ab; CZ: Qz.	240 Ma [72]; 258 Ma [38]	Biotite granite (270 Ma) [75]
Xiaokalasu	Xiaokalasu-Qiebielin	complex	spodumene	Li-Nb-Ta	WZ: Mc block and fine Ab-Qz-Ms-Grt-CGM; OIZ: Qz-Ms-Kf-Grt; IIZ: Spd-Qz-Ms-CGM and blocky Mc.	258–262 Ma [72]	Mica schist
Weizigou	Xiaokalasu-Qiebielin	beryl	beryl-columbite	Be	BZ: Qz-Ms-Tur; WZ: fine Ab-Qz-Ms-Grt-Brl; IZ: blocky Mc-Brl and coarse Qz-Ms-Brl-Tur block.	237 Ma [72]	Two mica granite (398–412 Ma) [76]
Taerlang	Xiaokalasu-Qiebielin			Barren	BZ: Kf-Qz-Ms-Bi-Grt-Tur; WZ: graphic intergrowth and Qz-Ms block	248 Ma [72]	Mica schist

Note: * represents muscovite Ar-Ar plateau ages and other ages of pegmatites are CGM or zircon U-Pb ages. BZ, border zone; WZ, wall zone; IZ, intermediate zone; OIZ, outer intermediate zone; IIZ, inner intermediate zone; CZ, core zone; MU, metasomatic unit; Ab, albite; Kf, K-feldspar; Mc, microcline; Qz, quartz; Ms, muscovite; Spd, spodumene; Brl, beryl; CGM, columbite-group minerals; Tur, tourmaline; Grt, garnet; Bi, biotite.

4. Samples and Analytical Methods

4.1. Samples

The following samples of muscovite from the Talate, Baicheng, Kangmunagong, Husite, Qunkuer, Dakalasu, Xiaokanasu, Weizigou and Taerlang pegmatite dykes were collected and studied. These samples are representative rocks from the barren pegmatites, Nb-Ta, Be, Be-Nb-Ta, Li-Nb-Ta and Li-Be-Nb-Ta pegmatites. The muscovites are assembled with columbite-group minerals in Nb-Ta pegmatite, with beryl in Be or Be-Nb-Ta pegmatites, and with spodumene in Li-Nb-Ta or Li-Be-Nb-Ta pegmatites. Descriptions of the samples are summarized in Table 2 and photographs are shown in Figure 2.

Table 2. Descriptions of the studied samples in the Chinese Altai.

Pegmatite Field	Pegmatite	Sample	Zone	Mineralogy Components
Qinghe	Talate (Li-Be-Nb-Ta)	12TLT-4	WZ	Ab (50)—Qz (25)—Ms (15)—Grt (2–5)—Brl (2–5)—CGM (2–5)
	Baicheng (Nb-Ta)	12TLT-7	CZ	Mc (45)—Ab (10)—Qz (30)—Ms (10)—CGM (5)
	Kangmunagong (Barren)	BC-2	Lens	Qz (70)—Ms (10)—Kf (10)—Ab (5)—Col-Tan (2–5)
Kelumute- Jideke	Qunkuer (Be)	KMNG-1		Kf (55–60)—Qz (25–30)—Ms (5–8)—Tur (5)—Grt (2)
	Husite (Be)	QKE-2-1		Qz (70)—Ms (15)—Ab (10)—Brl (5)
Dakalasu- Kekexier	Dakalsu (Be-Nb-Ta)	HST-5	IZ	Kf (45)—Qz (35)—Ms (10–15)—Brl (2–5)
	Xiaokalasu (Li-Nb-Ta)	HST-7	IZ	Kf (40)—Qz (45)—Ms (10)—Grt (2–5)
Xiaokalasu- Qiebielin	Xiaokalasu (Li-Nb-Ta)	DKLS-3	IZ	Kf (50–55)—Qz (10–15)—Ms(20)—CGM(5)—Brl(2–5)
	Weizigou (Be)	XKLS-2(2)	IZ	Ab (50–55)—Qz (15–20)—Spd (25)—Ms (5–10)
	Taerlang (Barren)	TEL-1(1)	WZ	Qz (60)—Mc (20)—Ms (10)—Brl (5)—Tur (2–5)
		WZG-4	IZ	Kf (40)—Qz (35–40)—Ms (15)—Bi (5)

Note: The numbers in brackets represent percent contents; BZ, border zone; WZ, wall zone; IZ, intermediate zone; CZ, core zone; Ab, albite; Kf, K-feldspar; Mc, microcline; Qz, quartz; Ms, muscovite; Spd, spodumene; Brl, beryl; CGM, columbite-group minerals; Tur, tourmaline; Grt, garnet; Bi, biotite. The samples KMNG-1, QKE-2-1 and WZG-4 are from [72].

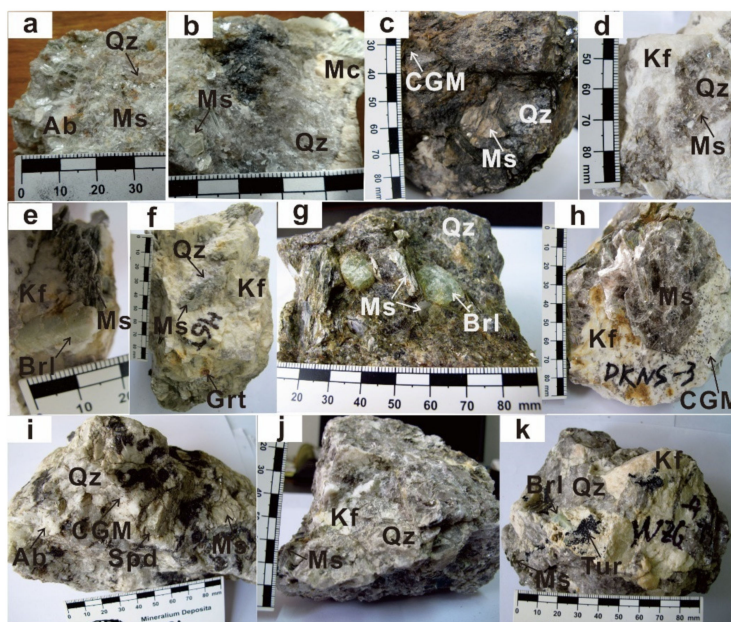


Figure 2. Photographs of samples (a) 12TLT-4, (b) 12TLT-7, (c) BC-2, (d) KMNG-1, (e) HST-5, (f) HST-7, (g) QKE-2-1, (h) DKLS-3, (i) XKLS-2(2), (j) TEL-1(1), (k) WZG-4. Ab, albite; Kf, K-feldspar; Qz, quartz; Ms, muscovite; Spd, spodumene; Brl, beryl; CGM, columbite-group minerals; Tur, tourmaline; Grt, garnet. Photos g and k are from [72].

4.2. Analytical Methods

4.2.1. EMPA

Major-element compositions of the minerals were determined using a JEOL JXA-8100 electron microprobe at the State Key Laboratory of Lithospheric Evolution, Institute of Geology and Geophysics, Chinese Academy of Sciences. An acceleration voltage of 15 kV and a beam current of 20 nA with beam diameters of 5 μm were used for quantitative analysis. The following standards were used for the quantitative analyses: Jadeite (Na-K α ; Al-K α), fluorite (F-K α), garnet (Fe-K α), pyrope (Mg-K α), diopside (Si-K α ; Ca-K α), bustamite (Mn-K α), rutile (Ti-K α), K-feldspar (K-K α), crocoite (Cr-K α) and ZnO (Zn-K α). Peaks and backgrounds were measured with counting times of 20 s or 40 s per element. The ZAF routine was used for data reduction [78]. The structural formula for muscovite was calculated on the basis of 24 anions, assuming stoichiometric amounts of H₂O as (OH), i.e., OH + F = 4 apfu (atoms per formula unit).

4.2.2. LA-ICP-MS

In situ trace element analyses of individual muscovite grains were determined using an Agilent 7500a ICPMS coupled to a 193 nm excimer ArF laser ablation system at the State Key Laboratory of Lithospheric Evolution, Institute of Geology and Geophysics, Chinese Academy of Sciences. The description of detailed analytical technique can be found in [79]. During analysis, spot size of 60 μm was applied with a repetition rate of 6 Hz, and the energy density employed was \sim 10 J/cm². All measurements were performed in time-resolved analysis mode utilizing peak jumping with 1 point per mass peak. Each spot analysis consisted of approximately 30 s of background acquisition and 60 s of sample data acquisition. NIST 612 was used as external standards, and mean Si values on individual grain determined by EPMA were used for internal calibration. Raw counts were processed offline and data-reduction and concentration calculations were then performed by Glitter [80].

5. Results

5.1. Major Elements

The mica of the pegmatites in the Chinese Altai analyzed here belongs to muscovite and phengite occasionally (Figure 3). The muscovite crystals analyzed are homogeneous in BSE images. The EMPA results of mica from the Talaite, Baicheng, Kangmunagong, Qunkuer, Husite, Dakalasu, Xiaokalasu, Taerlang and Weizigou pegmatite dykes are given in Supplementary Materials Table S1 and the representative data are shown in Table 3. The FeO contents vary from 0.54 wt% to 4.41 wt%. The MnO and MgO concentrations are in ranges below detection limit (bdl) –0.93 wt% and 0.01–1.12 wt%, respectively. The TiO₂ and F contents are bdl–1.42 wt% and bdl–1.16 wt%, respectively. The Na₂O contents are low (0.05–0.92 wt%), coupled with lower contents of ZnO (\leq 0.11 wt%), CaO (\leq 0.05 wt%) and Cr₂O₃ (\leq 0.04 wt%). The Li₂O contents based on the LA-ICP-MS data reach up to 0.36 wt%, whilst the calculated H₂O contents range between 3.89 wt% and 4.54 wt%, respectively.

5.2. Trace Components

The trace element compositions of muscovites in the pegmatite dykes analyzed here are given in Supplementary Materials Table S1 and the representative results are shown in Table 3. The large concentration variations occur in Li (82.7–1659 ppm), B (42.3–495 ppm), Sc (bdl–143 ppm), Ga (57.8–403 ppm), Rb (420–8329 ppm), Nb (33.9–343 ppm), Sn (bdl–800 ppm), Cs (6.40–2600 ppm), Ba (bdl–579 ppm) and Ta (1.27–243 ppm). Muscovite samples show smaller variations for Be (0.26–36.4 ppm), V (bdl–66.7 ppm) and W (0.56–80.7 ppm). Low concentrations are obtained for Ge (1.86–19.5 ppm), Sr (0.13–44.0 ppm), Pb (2.68–12.9 ppm), Co (0.06–7.33 ppm) and Zr (bdl–1.95 ppm, except 1 point of 1523 ppm), respectively. Lower contents are observed for Hf (bdl–1.15 ppm), Mo (bdl–0.34 ppm) and U (bdl–1.53 ppm), whilst the concentrations of REE, Y and Th are extremely low (bdl). The K/Rb, K/Cs and Nb/Ta ratios are in broad ranges of 10.4–196, 33.4–12761 and 0.73–26.68, respectively (Supplementary Materials Table S1).

Table 3. The representative EMPA and LA-ICP-MS results of muscovites in the pegmatite dykes of the Chinese Altai.

Pegmatite Dyke	Kangmunagong	Taerlang	Baicheng	Weizigou	Qunkuer	Husite	Dakalasu	Xiaokalasu	Talate		
Mineralization Type	Barren	Barren	Nb-Ta	Be	Be	Be	Be-Nb-Ta	Li-Nb-Ta	Li-Be-Nb-Ta		
Rock Type	Mc-Qz-Ms-Tur-Grt	WZ	Lens	IZ	Qz-Ms-Ab-Brl	IZ	IZ	IIZ	WZ	CZ	
Sample No.	KMNG-1	TEL-1(1)	BC-2	WZG-4	QKE-2-1	HST-5	HST-7	DKLS-3	XKLS-2(2)	12TLT-4	12TLT-7
/wt%											
SiO ₂	46.95	46.70	46.70	46.36	45.98	46.78	46.60	46.46	46.26	46.16	46.15
TiO ₂	0.12	0.51	0.03	1.29	0.07	bdl	0.09	0.23	0.03	0.34	0.41
Al ₂ O ₃	34.65	32.41	36.90	31.22	33.45	34.64	33.95	33.38	36.81	33.90	32.45
Cr ₂ O ₃	bdl	bdl	0.03	0.02	bdl	bdl	0.03	0.02	bdl	0.03	0.02
FeO	1.86	3.48	0.83	3.94	4.12	2.40	3.50	3.79	1.02	2.30	2.55
MnO	0.04	0.06	0.03	0.11	0.06	0.04	0.09	0.10	0.13	0.04	0.04
MgO	0.81	1.06	0.21	1.02	0.17	0.24	0.24	0.10	0.04	0.92	1.11
ZnO	bdl	0.02	0.07	0.04	0.04	bdl	bdl	0.07	0.05	0.08	0.08
CaO	bdl	bdl	0.02	bdl	bdl	bdl	0.02	0.02	bdl	0.02	0.04
Li ₂ O *	0.08	0.02	0.10	0.28	0.15	0.16	0.15	0.08	0.10	0.34	0.28
Na ₂ O	0.43	0.60	0.57	0.50	0.91	0.36	0.43	0.65	0.75	0.39	0.45
K ₂ O	10.11	9.84	9.83	9.52	9.62	9.96	9.59	9.41	9.52	10.13	10.39
F	bdl	bdl	0.33	0.46	1.16	0.24	0.47	0.51	0.08	0.76	0.82
O = F	bdl	bdl	0.14	0.20	0.49	0.10	0.20	0.21	0.03	0.32	0.35
H ₂ O *	4.50	4.44	4.39	4.19	3.87	4.36	4.24	4.19	4.47	4.10	4.02
Total	99.54	99.13	99.90	98.73	99.12	99.07	99.19	98.77	99.23	99.17	98.47
(O, OH, F) = 24											
Si	6.253	6.305	6.157	6.299	6.232	6.266	6.266	6.287	6.141	6.203	6.272
IVAl	1.747	1.695	1.843	1.701	1.768	1.734	1.734	1.713	1.859	1.797	1.728
IVSum	8.000	8.000	8.000	8.000	8.000	8.000	8.000	8.000	8.000	8.000	8.000
VIAI	3.694	3.464	3.892	3.299	3.577	3.737	3.648	3.612	3.902	3.572	3.471
Ti	0.012	0.052	0.003	0.132	0.007	0.000	0.009	0.023	0.003	0.034	0.042
Cr	0.000	0.000	0.003	0.003	0.000	0.000	0.003	0.002	0.000	0.003	0.002
Fe	0.207	0.393	0.092	0.447	0.467	0.269	0.394	0.429	0.113	0.258	0.290
Mn	0.004	0.007	0.004	0.012	0.007	0.004	0.010	0.011	0.015	0.005	0.005
Mg	0.160	0.214	0.042	0.206	0.034	0.047	0.047	0.020	0.009	0.184	0.224
Li	0.044	0.011	0.052	0.151	0.084	0.086	0.083	0.044	0.053	0.185	0.151
Zn	0.000	0.002	0.007	0.004	0.004	0.000	0.000	0.007	0.005	0.008	0.008
VISum	4.122	4.143	4.094	4.253	4.179	4.144	4.194	4.148	4.099	4.249	4.195
Ca	0.000	0.000	0.003	0.000	0.000	0.000	0.003	0.002	0.000	0.002	0.006
Na	0.111	0.156	0.145	0.131	0.239	0.093	0.111	0.171	0.193	0.101	0.118
K	1.717	1.695	1.654	1.650	1.664	1.702	1.645	1.625	1.612	1.736	1.802
XIISum	1.828	1.852	1.802	1.781	1.903	1.794	1.759	1.799	1.805	1.839	1.927
F	0.000	0.000	0.138	0.199	0.498	0.100	0.198	0.217	0.034	0.324	0.354
OH	4.000	4.000	3.862	3.801	3.502	3.900	3.802	3.783	3.966	3.676	3.646

Table 3. Cont.

Pegmatite Dyke	Kangmunagong	Taerlang	Baicheng	Weizigou	Qunkuer	Husite	Dakalasu	Xiaokalasu	Talate		
Mineralization Type	Barren	Barren	Nb-Ta	Be	Be	Be	Be-Nb-Ta	Li-Nb-Ta	Li-Be-Nb-Ta		
Rock Type	Mc-Qz-Ms-Tur-Grt	WZ	Lens	I _Z	Qz-Ms-Ab-Brl	I _Z	I _Z	I _{IIZ}	WZ	CZ	
Sample No.	KMNG-1	TEL-1(1)	BC-2	WZG-4	QKE-2-1	HST-5	HST-7	DKLS-3	XKLS-2(2)	12TLT-4	12TLT-7
/ppm											
Li	385	94.7	453	1279	717	745	716	380	461	1591	1287
Be	0.401	5.53	24.8	26.0	20.5	23.1	21.3	27.0	22.59	25.5	23.7
B	82.2	60.1	382	78.9	71.3	133	131	146	141	86	307
P	134	23.8	175	28.1	126	58.9	38.0	58.5	53.3	139	145
Sc	22.9	99.5	1.7	66.7	1.86	2.11	1.36	4.48	2.19	8.79	3.94
V	0.033	36.1	28.3	43.0	0.151	0.334	3.18	4.05	1.47	47.3	21.1
Mn	172	536	264	781	320	744	812	617	908	311	246
Co	0.317	1.32	0.79	1.36	0.070	0.197	0.324	0.282	0.08	6.66	5.14
Ga	60.0	145	67.3	112	120	114	124	388	122	72.1	67.7
Ge	2.82	2.27	13.8	3.84	4.28	3.71	4.58	6.79	6.01	9.08	19.5
Rb	428	455	4434	1205	4015	2963	2964	3843	4733	4774	8329
Sr	3.21	16.3	6.54	9.34	1.12	3.53	0.515	0.266	3.07	3.75	4.2
Zr	1523	1.61	bdl	1.18	0.393	0.308	1.08	1.121	bdl	0.73	0.237
Nb	40.3	86.3	170	122	301	257	305	169	159	231	300
Mo	0.112	0.324	bdl	0.087	bdl	0.176	0.096	0.092	bdl	0.093	bdl
In	0.197	0.996	bdl	0.31	0.256	0.123	0.045	4.86	0.079	0.069	0.021
Sn	12.4	34.7	bdl	15.8	62.3	21.2	9.60	773	18.1	1.73	0.92
Cs	7.69	6.4	472	100	93.5	107	101	517	280	332	1514
Ba	6.57	315	5.08	252	bdl	1.39	1.41	1.24	2.85	82.5	28.3
Hf	0.27	bdl	bdl	0.14	bdl	bdl	0.195	0.826	bdl	0.51	0.133
Ta	1.86	3.77	58.1	26.7	24.5	16.1	24.7	225	46.8	53.9	109
W	22.5	78.2	0.94	17.0	31.6	17.6	16.8	57.3	5.81	5.99	1.62
Pb	7.4	6.88	5.63	6.33	4.62	5.08	4.5	12.1	4.9	2.96	4.14
Th	bdl	bdl	bdl	0.032	bdl	0.016	bdl	bdl	bdl	bdl	bdl
U	bdl	bdl	bdl	1.53	0.082	bdl	bdl	bdl	bdl	bdl	bdl
K/Rb	195.77	179.65	18.40	65.55	19.89	27.87	26.84	20.32	16.68	17.60	10.35
K/Cs	10,904	12,761	173	786	854	769	786	151	282	253	56.95
Li/Cs	50.06	14.80	0.96	12.74	7.67	6.93	7.07	0.73	1.64	4.80	0.85
Nb/Ta	21.69	22.90	2.92	4.56	12.28	15.93	12.37	0.75	3.40	4.28	2.75

Note: bdl, below detection limit; *, calculated using LA-ICP-MS data; WZ, wall zone; I_Z, intermediate zone; I_{IIZ}, inner intermediate zone; CZ, core zone; Ab, albite; Mc, microcline; Qz, quartz; Ms, muscovite; Brl, beryl; Tur, tourmaline; Grt, garnet.

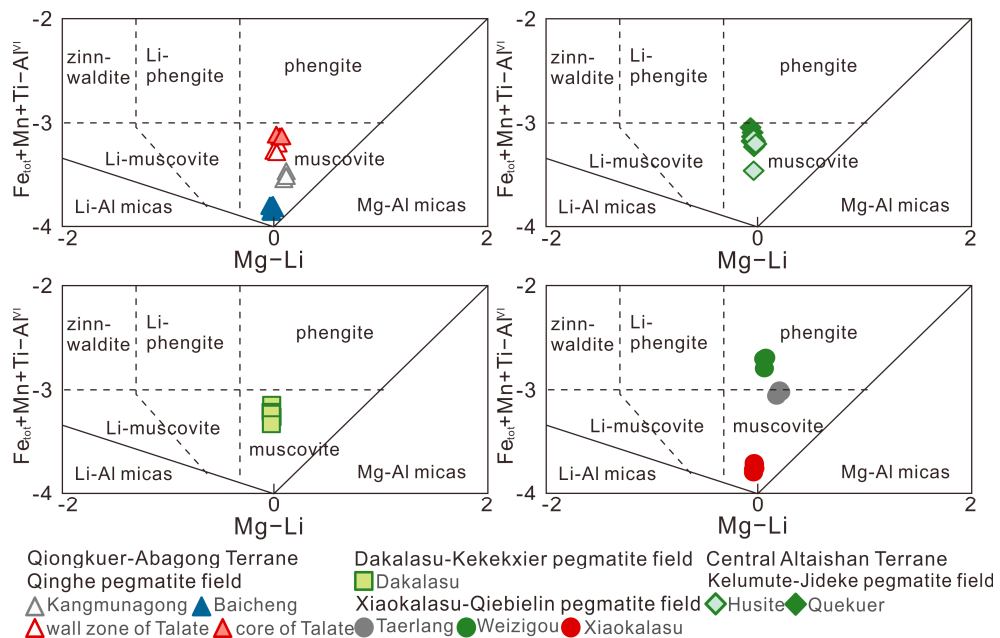


Figure 3. Mg-Li vs. $\text{Fe}_{\text{tot}} + \text{Mn} + \text{Ti-Al}^{\text{VI}}$ diagram according to [81].

6. Discussion

6.1. Substitutions among Alkali Elements

Li, Rb and Cs are important alkali elements incorporated in muscovite since the contents of Li, Rb and Cs of muscovite generally increase during the progressive fractionation process of pegmatite dyke. In the Chinese Altai, from the barren to REL pegmatite dykes, Rb and Cs basically display a positive correlation with Li and these alkali elements are more incorporated in muscovites. It is believed that Li^+ substitute for Al^{3+} at the octahedral site [82] and the incorporation of Li into Al-rich/dioctahedral micas appears to be controlled by the substitutions $\text{Si}_{+2}\text{Li}_{+1}\text{Al}_{-3}$, $\text{Li}_{+3}\text{Al}_{-1}\square_{-2}$ [13], $\text{Li}_{+1}\text{Fe}_{+1}\square_{-1}\text{Al}_{-1}$, $\text{Li}_{+2}\text{Si}_{+1}\text{Al}^{\text{VI}}_{-1}\text{Al}^{\text{IV}}_{-1}$, and $\text{Fe}_{+1}\text{Mg}_{+1}\text{Mn}_{+1}\text{Li}_{+1}\text{Al}^{\text{VI}}_{-1}\square_{-1}$ [83]. Here, a negative correlation between Li and Al^{VI} and a positive correlation between Li and total Fe, Mg and Mn (Figure 4) suggest that Li^+ accompanied with Fe, Mg and Mn substitute for Al^{3+} at the octahedral site. In general, Rb and Cs come into the interlayer site on account of large atomic radius [84]. In some of the Be pegmatites, Rb is negatively related to Cs and Li (Figure 4). The atomic radius of Li is obviously smaller than those of Rb and Cs, but Rb and Cs have similar atomic radius. Thus, there might be a substitution of Rb by Cs at interlayer space in muscovite from some of the Be pegmatites. In the Li-mineralized pegmatite dykes (Li-Nb-Ta and Li-Be-Nb-Ta pegmatites), Rb and Cs concentrations decrease and Li contents increase (Figure 4). Rb and Cs in muscovite might not be directly substituted by Li on account of difference concerning atomic radius. It is noted that muscovites in Li-mineralized pegmatite show trends of relatively high Al^{VI} and low total Fe, Mn and Mg (Figure 4). Therefore, large amount of Li incorporation in muscovites from Li-mineralized pegmatite might be also related to other substitution mechanisms which involve the reduction of Rb and Cs in muscovite in some degree.

6.2. Implications of Fluxes and HFSE

Enrichment of fluxes (i.e., F, B and P) is an important feature for pegmatite magma because they favor the pegmatitic textures (i.e., graphic pegmatite UST, or giant crystals) and REL mineralization [85,86]. The concentrations of F and P of muscovite show a positive correlation with the Li and Cs contents, which are indicators of evolution degree (Figure 5). Fluxes (i.e., F and P) were mostly collected in pegmatite magmas with a high degree of fractionation. A positive correlation between P and B could be identified in

Figure 5. The contents of P and B are basically positively related to evolution degree, but the quartz-muscovite-columbite-tantalite lens of the Baicheng Nb-Ta pegmatite with a middle evolution degree are obviously enriched in P and B (Figure 5), suggesting that fluxes (i.e., B and P) accumulated at late fluid-rich stage during pegmatite evolution compared to other zones of pegmatite.

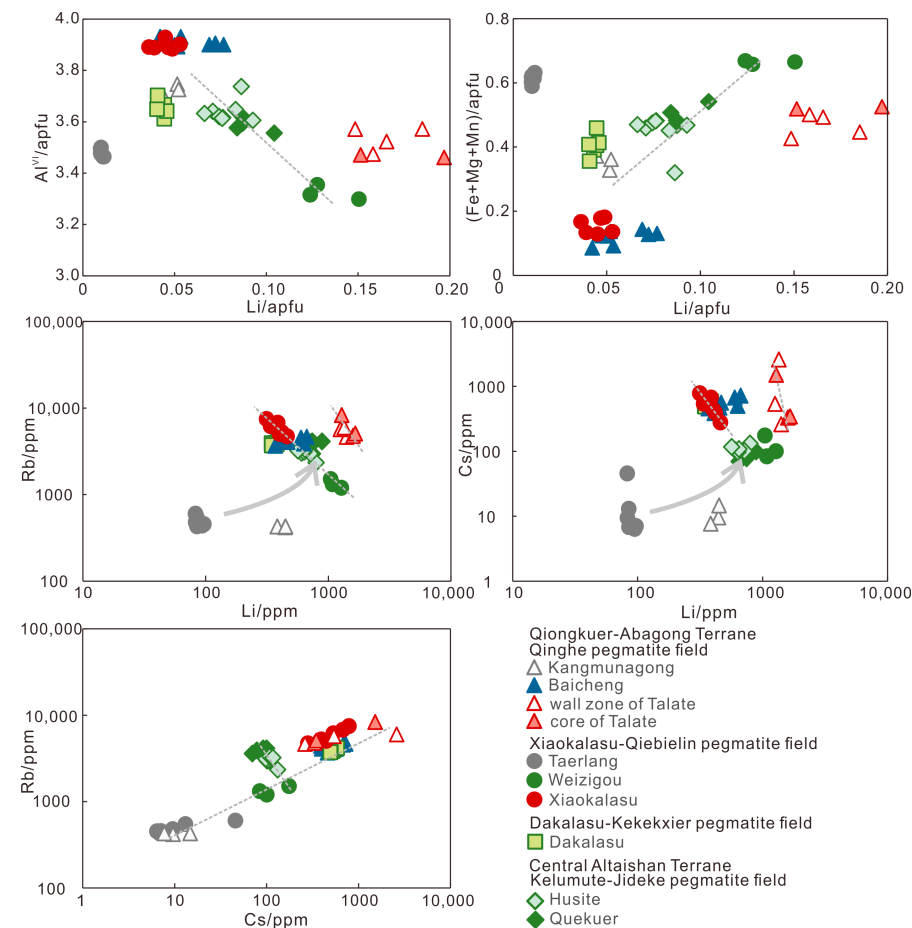


Figure 4. Plots of Fe + Mg + Mn, Al^{VI} vs. Li apfu, Rb, Cs vs. Li and Rb vs. Cs contents showing substitutions among alkali elements.

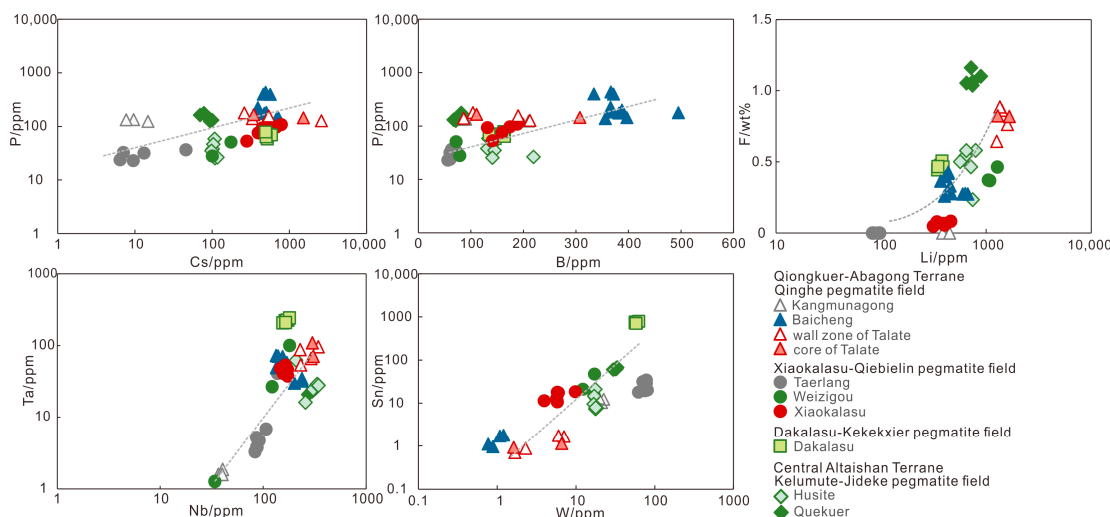


Figure 5. Plots of P vs. Cs and B, F vs. Li, Ta vs. Nb and Sn vs. W contents.

Muscovite is mainly considered as a repository of Sn, Nb, Ta and W in evolved granitic rocks [87,88]. From barren to REL pegmatites, muscovites generally show higher Nb and Ta contents. The enrichment of both Nb and Ta of muscovites is possibly affected by highly evolved pegmatite magma. Due to the differences of partition coefficients of Nb and Ta and the presence of large amounts of Nb-Ta bearing phases, the correlation between Nb and Ta in muscovite among the REL pegmatites becomes complicated. There is a positive correlation between Sn and W, reflecting their similar behaviors in the pegmatite systems, and a weakly negative correlation between concentrations of Sn and W and evolution degree of magma can be seen (Figure 5), indicating that Sn and W contents might be related to fractional crystallization, fluid activities or other factors such as magma source [26,89–91]. Here, muscovites in the Dakalasu Be-Nb-Ta pegmatite are extremely enriched in Nb, Ta, W and Sn, mainly controlled by chemical features of magma, which is a Nb-Ta-Sn-W-rich pegmatite-forming magma [92], supported by occurrences of cassiterite and W-columbite-tantalite in the Dakalasu (Be-Nb-Ta) pegmatite (WO_3 up to 4.31 wt% [72]).

6.3. The Evolution Degree of Different REL Pegmatites

It is believed that different REL mineralization types are controlled by evolution degree of pegmatite magma [93–95]. The indicators of evolution degree in mica include the K/Rb and K/Cs values [21], and the contents of Li [20], Rb, Cs [13,14] and F [22,24]. With increase of degree of evolution of pegmatites, the K/Rb and K/Cs values decrease and the contents of Li, Rb, Cs and F increase. The K/Rb value and Cs content of muscovites are relatively reliable indicators of evolution degree of pegmatite magma [7,18,19,24,25,27]. Plot of K/Rb vs. Cs is used to discriminate REL mineralization types of pegmatites [84,93,96]. The muscovite samples come from barren pegmatite, lens saturated in columbite group minerals (CGM) from Nb-Ta pegmatite, zones saturated in beryl from Be pegmatite, zones assembled with beryl and CGM from Be-Nb-Ta pegmatite, and zones saturated in spodumene from Li-Nb-Ta pegmatite. According to the consistent ranges of K/Rb ratios and Cs contents, there is no evidently fractional crystallization from the wall zone to core of the Talate Li-Be-Nb-Ta pegmatite dyke. Thus, the muscovites from these zones could reflect the chemical features of magma that formed the inner intermediate zone, which is saturated in beryl and spodumene. Moreover, muscovites from the Koktokay No.3 Li-Be-Nb-Ta-Rb-Cs pegmatite deposit in the Chinese Altai, which consists of nine zones and experienced three stages accompanied with Be-Nb-Ta, Li-(Be)-Nb-Ta and (Li-Ta-)Rb-Cs deposition [46,97–100], are added to discuss the evolution degree of REL pegmatites in this region and the data are from [45]. The compositions of these muscovites reflect the chemical features of pegmatite-forming magma that are at equilibrium of different REL minerals (beryl, spodumene, CGM and lepidolite) for pegmatites with diverse REL mineralization, respectively.

Overall, from barren pegmatite, the beryl-bearing zone, to the spodumene-bearing zone, the pegmatite-forming magma basically display an increasing evolution degree due to decreasing K/Rb ratios and increasing Cs contents (Figure 6). This is in accordance with the previous studies of other pegmatite fields (e.g., Totoral pegmatite field, Argentina [93]). The muscovites from the beryl-bearing zones of the Li-Be-Nb-Ta-Rb-Cs pegmatite (zones I–IV) have close K/Rb ratios and Cs concentrations compared to those from the Be-mineralized pegmatite dykes (Be and Be-Nb-Ta pegmatites) (Figure 6). It is noted that the muscovites from the lens of Nb-Ta pegmatite dyke and beryl-bearing zones in Be-Nb-Ta pegmatite display a similar evolution degree of magma, but host higher Cs contents than beryl-bearing zones in single Be pegmatite (Figure 6). This might be related to more fluid at formation of these zones, accompanied with higher fluxes and elevated amounts of Ta [101,102]. Similarly, spodumene-bearing zones of the Li-Be-Nb-Ta-Rb-Cs pegmatite (zones V–VI) show close K/Rb ratios but higher Cs concentrations than those zones from Li-Nb-Ta and Li-Be-Nb-Ta pegmatites (Figure 6). Finally, the lepidolite-bearing zone of the Li-Be-Nb-Ta-Rb-Cs pegmatite (zone VIII) displays higher evolution degree than spodumene-bearing zones of the Li-mineralized pegmatites (Figure 6).

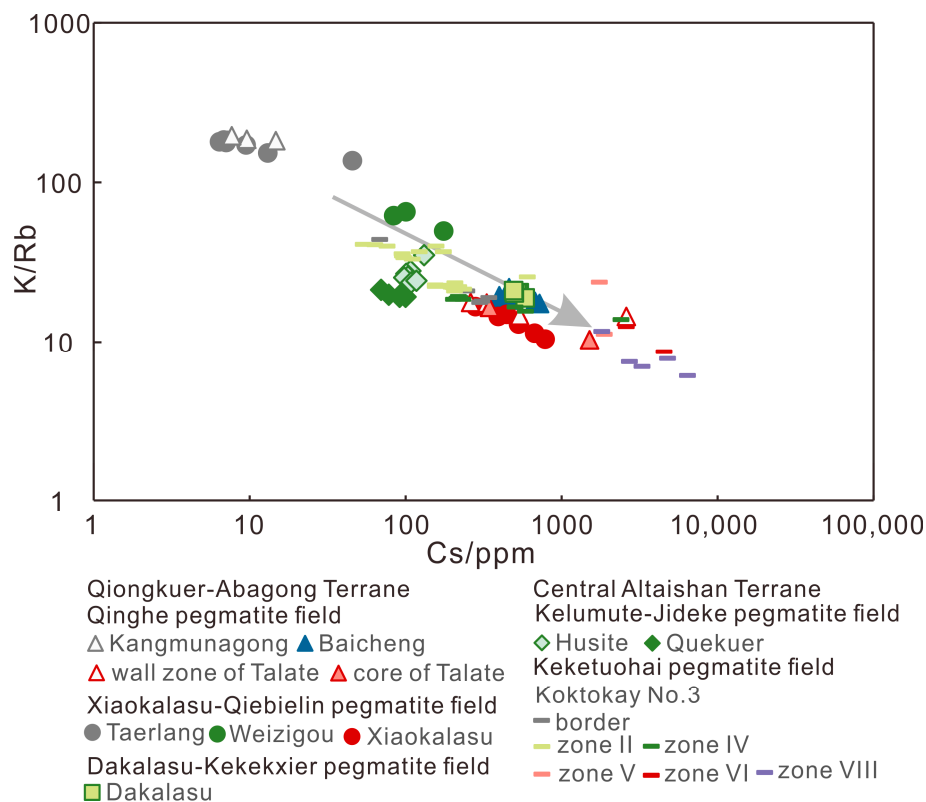


Figure 6. Plot of K/Rb vs. Cs content for muscovites from the pegmatites studied and the Koktokay No.3 pegmatite in the Chinese Altai. The regions of zones I–IV and zones V–VIII of the Koktokay No.3 pegmatite are based on the data from [45,100].

6.4. Possible Indicators of Different REL Mineralization

The chemical compositions of minerals are mainly controlled by characteristics of forming liquid, elements partition for mineral/melt and mineral/mineral and crystal structures. The trace element incorporations into muscovite on accounts of flexibility of crystal structure supply an opportunity to look for possible indicators of different REL mineralization and further be good for REL prospecting to some extent.

(1) Barren, Be-mineralized and Li-mineralized pegmatites

Compared to the zones saturated in REL minerals from different pegmatite dykes with diverse REL mineralization types, muscovites from barren pegmatites are strongly poor in Rb (ca. 400–600 ppm), Cs (ca. 5–50 ppm), Ge (<3 ppm), Ta (<10 ppm), Be (<10 ppm) and F (negligible in EMPA), and relatively rich in MgO (~1 wt%) (Figure 7). In comparison with barren pegmatite and zones saturated with Li-silicate minerals from Li-mineralized pegmatites, muscovites intergrown with beryls from Be-mineralized pegmatite dykes host middle concentration levels of Rb (ca. 1200–4000 ppm), Cs (ca. 100–500 ppm) and Ge (ca. 4–6 ppm) and a high content level of FeO (ca. 3–4 wt%) (Figure 7). The muscovites from the Li-mineralized pegmatites have contents of Rb (>4500 ppm), FeO (ca. 1–2.5 wt%) and large variations of Cs (>300 ppm), and Ge (ca. 6–12 ppm) (Figure 7). While Li concentration of muscovite exceeding 600 ppm [103] or 500 ppm [82] was suggested as an indicator for the identification of spodumene-rich pegmatites, the muscovites from the Xiaokalasu Li-Nb-Ta pegmatite are relatively poor in Li and those from the Be pegmatites are rich in Li. Moreover, no consistent correlation can be seen between the Li content of muscovite and the presence of spodumene in spodumene-rich Moflan pegmatite [9,82]. Thus, Li content of muscovite might not be a reliable indicator of spodumene-bearing pegmatite in the Chinese Altai.

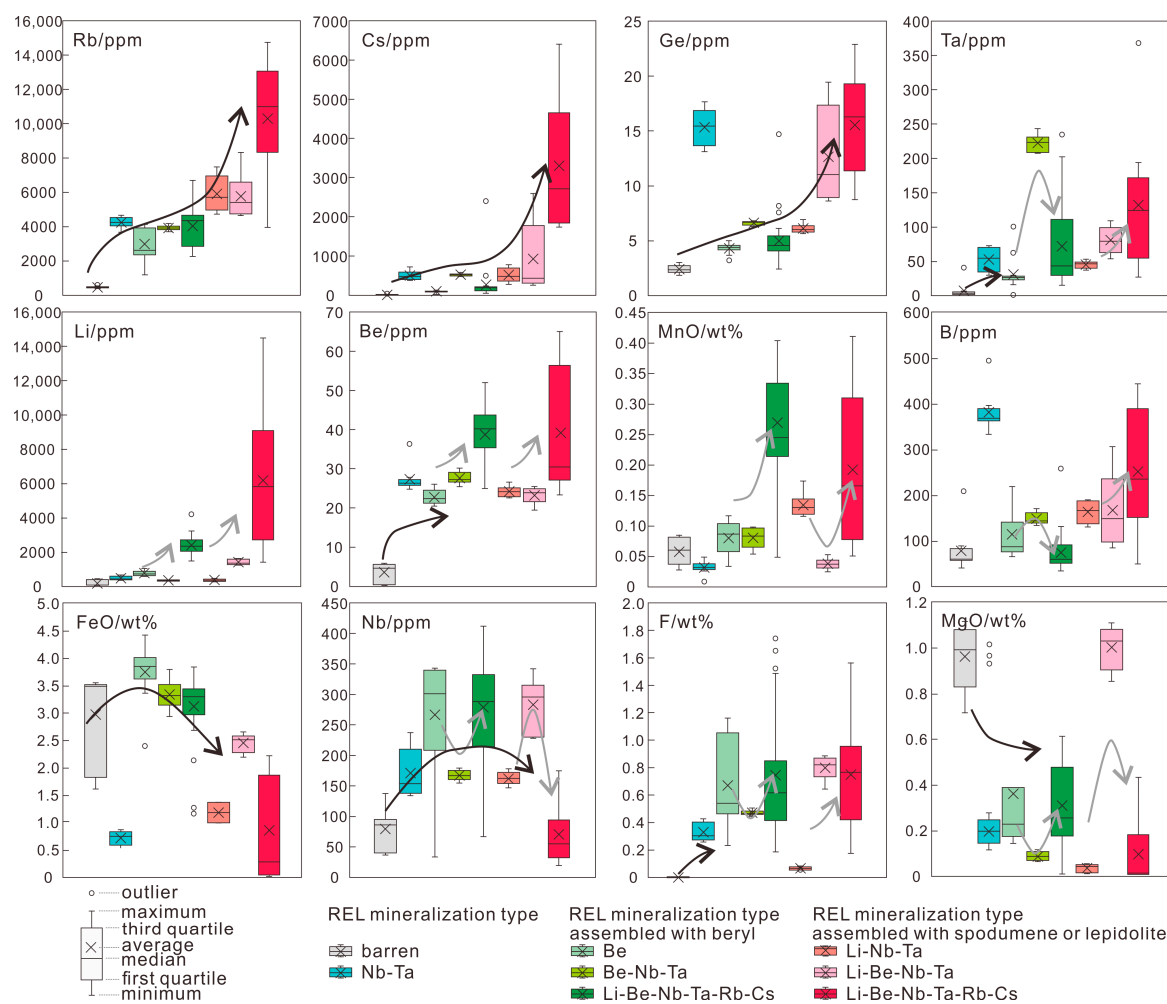


Figure 7. Whisker-box diagrams of variations of Rb, Cs, Ge, Ta, Nb, Li, Be, B, F, FeO, MnO and MgO contents, showing compositional trends of muscovites from pegmatites with diverse REL mineralization types. The Koktokay No.3 pegmatite represent the Li-Be-Nb-Ta-Rb-Cs mineralization type and zones I–IV and V–VIII are related to those assembled with beryl and spodumene/lepidolite, respectively. The data of muscovites of the Koktokay No.3 pegmatite are from [45,100]. The black and grey arrows represent trends of changes from barren to Li-Be-Nb-Ta-Rb-Cs pegmatite and among beryl-bearing or spodumene-bearing pegmatites, respectively.

(2) Nb-Ta-, beryl- and spodumene-(lepidolite)-bearing pegmatites

The lens of Nb-Ta pegmatite reveals the specific features of muscovite crystallizing from late fluid during Nb-Ta-bearing pegmatite evolution, including high B (334–495 ppm) and Ge (13.1–17.7 ppm) and low FeO (<1 wt%) contents (Figure 7). Compared to those of Be pegmatite, muscovite saturated with beryls from the Be-Nb-Ta pegmatite display extremely high contents of Ta, Cs and low contents of Li, Nb and FeO (Figure 7), reflecting the chemistry characteristics of Ta-rich pegmatite-forming magma and effected by large amounts of CGM crystallization. The muscovites assembled with spodumene from the Li-mineralized pegmatites are in consistent concentrations of Rb and Be, but those from the Li-Be-Nb-Ta pegmatite are rich in Cs, Ge, Nb, Ta, Li, F, MgO and FeO and poor in MnO (Figure 7). Both evolution degree of magma and features of magma for a single pegmatite dyke have effects on muscovite chemistry. The muscovites from zones I–IV and zones V–VIII of the Li-Be-Nb-Ta-Rb-Cs pegmatite have obviously higher contents of Li, Be and MnO than those from beryl-bearing and spodumene-bearing zones of other Be-

and Li-mineralized pegmatites, respectively (Figure 7) [45], indicating a highly evolved pegmatite magma at emplacement.

On the basis of comparisons summarized above, some trace elements show evidential differences among diverse REL mineralization types, such as Rb, Cs, Ge, Ta, etc. The Nb/Ta ratios of muscovite are also different among the pegmatites with distinct REL mineralization types (Figure 8). The Nb/Ta values of muscovite normally decrease with an increasing evolution trend due to preferential incorporation of Nb in muscovite and columbite [27,104], lower solubility of columbite-(Mn) than tantalite-(Mn) in peraluminous granitic melts [104,105] and an enrichment of Ta relative to Nb in residual liquids [106]. The tantalite crystallization caused by supersaturation at strong undercooling [107] would make an effect on the Nb/Ta ratios. The muscovites from zone II of the Koktokay No.3 pegmatite display various Nb/Ta ratios, some of which overlap those of the Li pegmatites (Figure 8). The Nb and Ta contents of pegmatite magma also play roles in Nb/Ta ratios. The Dakalasu Be-Nb-Ta pegmatite has a middle evolution degree, but the muscovites show lower Nb/Ta ratios (Figure 8). The Nb/Ta ratios of muscovite generally change with evolution degree of magma and are scattered in some degree. Thus, combined with the K/Rb ratio and Cs content that are accepted indicators of fractionation [27], we propose potential plots of Nb/Ta vs. Cs and K/Rb vs. Ge to discriminate barren, Be- and Nb-Ta-(Li-Be-Rb-Cs)-bearing pegmatites (Figure 8).

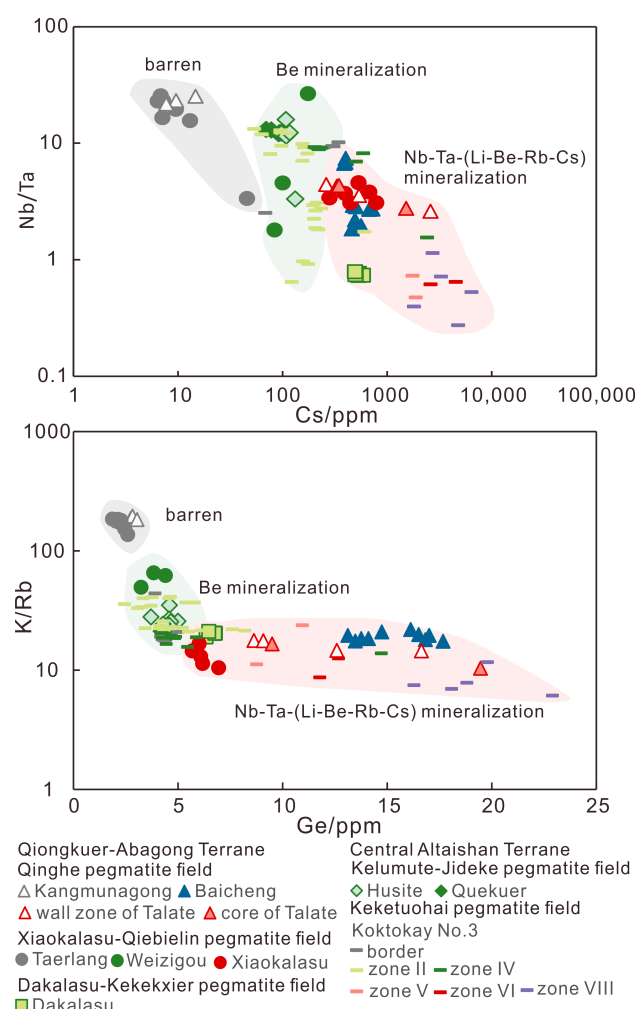


Figure 8. Variation diagrams of Nb/Ta vs. Cs content and K/Rb vs. Ge content, indicating the differences of muscovites from the barren, Be and Nb-Ta-bearing pegmatites in the Chinese Altai. The regions of zones I–IV and zones V–VIII of the Koktokay No.3 pegmatite are based on the data from [45,100].

6.5. Evaluation of the REL Concentrations of Liquids

The use of mineral composition and melt/mineral partition provides a semi-quantitative estimate of melt trace element contents during crystallization [27]. Micas offer better perspectives than feldspars that are easily re-equilibrated at low temperatures [108] and quartz that are generally very pure except for only a few trace elements [109]. Considering temperatures of pegmatite formation (620–700 °C) and saturation/trace level of rare elements (Li, Be, F, Rb and Cs), the partition coefficients $D^i_{\text{ms}/\text{melt}}$ (i = incompatible trace element) [10,110,111] are preferred as values in Supplementary Materials Table S2. The muscovite crystals analyzed here are from barren pegmatite or intergrown with Be- or Li-aluminosilicate crystals in REL pegmatite. The calculated trace element contents of liquids (referring to forming medium for minerals) at equilibrium with these muscovites reflect the characteristics of trace elements of barren pegmatite-forming magma or REL-enriched magma with different REL mineralization types.

Overall, the calculated trace element concentrations for liquid (pegmatite melt) are close or similar to the reported data of those inferred for pegmatite melts (Table S3) (Li, 0.5–1.0 wt% 3000–10000 ppm, [85,112,113]; Be, 25–70 ppm, [111]; F, ca. 1–2 wt%, [85,113]; Rb, 0.05–0.15 wt%; Cs, 0.01–0.02 wt%, [27]). $\text{Rb}_{(\text{liq})}$ and $\text{Li}_{(\text{liq})}$ define correlation, respectively, positive with $\text{Cs}_{(\text{liq})}$ as expected for pegmatite differentiation [114,115] and no clear correlation between $\text{Be}_{(\text{liq})}$, $\text{F}_{(\text{liq})}$ and $\text{Cs}_{(\text{liq})}$ could be seen (Figure 9). The liquids of the barren and REL pegmatite dykes in the Chinese Altai calculated by muscovite (Supplementary Materials Table S3) display Be contents of <5 ppm and ca. 15–50 ppm. The liquids of the barren and spodumene-absent REL pegmatites show Li contents of ca. 400–2300 ppm and >1800–6000 ppm (Supplementary Materials Table S3). The magmas that produce beryl and CGM host more Be and Li contents than barren pegmatites. Fractional crystallization contributes to Be and Li accumulation in pegmatite magma.

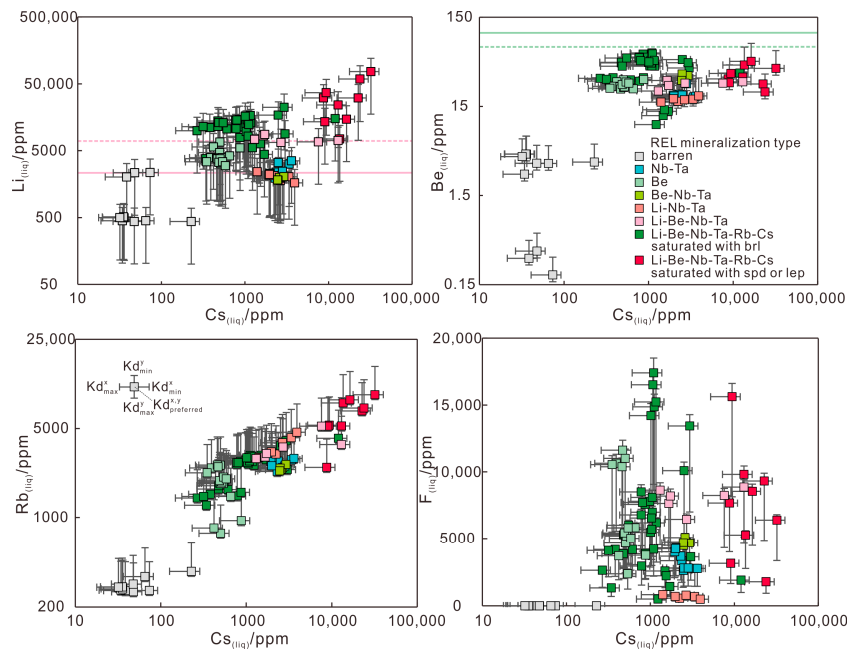


Figure 9. Calculated trace element contents (Li, Be, F and Rb) of liquids at equilibrium with muscovite from REL pegmatite dykes plotted as a function of the calculated Cs concentration of the liquid. The Koktokay No.3 pegmatite represents the Li-Be-Nb-Ta-Rb-Cs mineralization type and the compositions of muscovites from zones I–IV and V–VIII [45,100] are used for calculating the trace elements content of liquids that are saturated with beryl and spodumene/lepidolite, respectively. The green dashed and solid lines refer to Be contents of liquid saturated with beryl and beryl-bearing pegmatite [111]. The pink dashed and solid lines indicate Li contents of liquid saturated with Li-aluminosilicate and spodumene-bearing pegmatite [112,116].

6.5.1. Be Content of Beryl-Forming Magma for Be-Mineralized Pegmatite

The average Be contents of crust and granitic rocks are ~2 ppm and ~5 ppm, respectively [111]. Be contents of pegmatites have been estimated ranging from ~35 to ~575 ppm Be [111,117–119]. Beryl-bearing pegmatites contain >100 ppm Be and beryl-rich pegmatites have an average Be content of 230 ppm [111]. Be contents of pegmatites increase from beryl- to spodumene- and lepidolite-bearing pegmatites [111], since the solubility of beryl in melt with speciation reactions involving Li, F, B and P is greater [120]. It is inferred that a beryl-bearing pegmatite initially contains 140 ppm Be [121]. Silicic melts become saturated in beryl with as little as ~70 ppm Be [120]. Extended fractionation beyond ~95% total solidification by at least a three-step process is required to achieve beryl saturation in granite magmas [111]. Therefore, a high evolution degree of magma is required to achieve enough Be content in magma for the presence of beryl.

It is noted that the Be contents of the liquids at equilibrium with beryl in the Chinese Altai are commonly lower than the ~70 ppm (Figure 9) required for beryl saturation in silicic melts [120]. The beryl-bearing pegmatites investigated in this study show a relatively high evolution degree that is similar to those of Be-mineralized pegmatites (Figure 6) [93]. Thus, besides a higher evolution degree, there is another factor that could control beryl saturation. The solubility of beryl falls with decreasing temperature [120] and Be content of melt decreases with a lower temperature [111]. Temperature is an important control on beryl deposition, because BeO content of melt projects to a narrow range of similar values at low T and metaluminous to peraluminous granitic magmas with/without volatile and fluxing components will have similarly low BeO requirements for beryl saturation, if cooled to subsolidus temperatures [120]. This is the major reason why the BeO content of pegmatite-forming liquid for the beryl-bearing pegmatite rocks in the Chinese Altai is relatively low. Both highly evolved pegmatite magma and low temperature at emplacement are important factors for beryl formation in the REL pegmatites in the Chinese Altai.

6.5.2. Li Content of Spodumene-Forming Magma for Li-Mineralized Pegmatite

The average Li content of crust ranges from 13 to 35 ppm [122,123]. The average content of Li for the spodumene-bearing pegmatites is ~2323 ppm [112]. The Li-rich pegmatite magma come from extremely high fractionation of evolved granitic magma [95,124,125], low-degree partial melting [126] or exsolution of supercritical fluid enriched in alkalis and fluxes [127]. Granitic melts become saturated in spodumene with as little as ~6968 ppm Li, but Li-aluminosilicate would not crystallize until the system experienced a delay to accumulate thousands of ppm Li in the melts above the saturation value and supersaturation in the melt was achieved [116]. The liquids saturated with spodumene of the Li-Nb-Ta, Li-Be-Nb-Ta and Li-Be-Nb-Ta-Rb-Cs pegmatites in the Chinese Altai contain >1600 ppm, >6600 ppm and >24,000 ppm Li (Supplementary Materials Table S3). Compared to the Li saturation value, the Li contents of liquid of the Xiaokalusu Li-Nb-Ta are very low and those of the Talate Li-Be-Nb-Ta are close but could not reach up to Li supersaturation (Figure 9). However, the spodumene assembled with these muscovites in the same zone of pegmatites occurred. There are some possibilities. (1) When the Li supersaturation is achieved or nearly achieved, further cooling or Li-poor phase crystallization are required for initial spodumene crystallization [116,128]. Muscovite as one of the ‘Li-poor’ phases ($K_{d,Li} = 0.12\text{--}0.82$) formed, reflecting the state of melts at Li saturation or unsaturation. Thus, muscovite with low Li content occurs with spodumene. (2) The low Li content of liquid with spodumene saturation might be related to heterogeneous distribution of lithium. The boundary layers concentrate incompatible and fluxing components (e.g., Li and F) and further form Li-aluminosilicate [4,85,129]. Muscovites do not form by boundary layers. This is in accordance with low F contents of liquid of Li-Nb-Ta pegmatite (Figure 9). On the other hand, from the spodumene-glass interface to >200 μm outside, the Li concentrations of liquid could decrease from ~6000 to ~1600 ppm in the dissolution experiments [116]. The liquids outside spodumene crystals are not so rich in Li, leading to muscovite with

lower Li contents. Thus, taking Li content of muscovite as a tracer for REL mineralization is in need of more investigation.

7. Conclusions

The chemistry of muscovites from the pegmatites of the Chinese Altai reveals that the pegmatite magmas for barren, Nb-Ta, Be, Be-Nb-Ta, Li-Nb-Ta and Li-Be-Nb-Ta are complex and diverse. The chemical studies of muscovite contribute to looking for REL mineralization type tracers and reflecting the ore-forming process in some degree.

1. Li⁺ accompanied with Fe, Mg and Mn substitute for Al³⁺ at the octahedral site in muscovite from the REL pegmatite in the Chinese Altai. The muscovite from some of the Be pegmatites shows a substitution of Rb by Cs at interlayer space.
2. The lenses of the Baicheng Nb-Ta pegmatite are produced at late fluid-rich stage with high fluxes including P and B. The enrichment of HFSE in muscovite indicates a Nb-Ta-Sn-W rich pegmatite magma for the Dakalasu Be-Nb-Ta pegmatite.
3. From barren pegmatite, beryl-bearing zone, to spodumene-bearing zone, the pegmatite-forming magma basically display an increasing evolution degree.
4. The possible indicators of muscovite for barren, Be- and Li-mineralized pegmatites mainly controlled by evolution degree are summarized. In the Chinese Altai, the muscovites from barren pegmatites contain ca. 400–600 ppm Rb, ca. 5–50 ppm, and Cs <3 ppm Ge with <10 ppm Ta and <10 ppm Be; those intergrown with beryl have ca. 1200–4000 ppm Rb, ca. 100–500 ppm Cs, ca. 4–6 ppm Ge and ca. 3–4 wt% FeO; those assembled with spodumene host >4500 ppm Rb, ca. 6–12 ppm Ge and ca. 1–2.5 wt% FeO with large variations of Cs (>300 ppm). The plots of Nb/Ta vs. Cs and K/Rb vs. Ge are proposed to discriminate barren, Be- and Nb-Ta-(Li-Be-Rb-Cs) pegmatites.
5. The Li, Be, Rb, Cs and F concentrations of liquid were evaluated using the trace element compositions of muscovites from barren and REL pegmatites in the Chinese Altai. The high Rb and Cs contents of liquid and lower Be contents than beryl saturation value indicate that both highly evolved pegmatite magma and low temperature at emplacement contribute to beryl formation. The liquids saturated with spodumene have large variations of Li, possibly related to metastable state at Li unsaturation-supersaturation or heterogeneous distribution of lithium in the system.

Supplementary Materials: The following are available online at <https://www.mdpi.com/article/10.3390/min12030377/s1>, Table S1: The EMPA and LA-ICP-MS results of muscovites from the pegmatite dykes in the Chinese Altai. Table S2: Muscovite/melt partition coefficients (Kd) used in this study. Table S3: The calculated Li, Be, F, Rb and Cs contents of liquids at equilibrium with muscovites from the pegmatite dykes in the Chinese Altai.

Author Contributions: Conceptualization, Q.Z. and K.Q.; methodology, Q.Z. and D.T.; software, Q.Z.; validation, D.T.; formal analysis, Q.Z.; investigation, Q.Z., D.T. and C.W.; data curation, Q.Z.; writing—original draft preparation, Q.Z.; writing—review and editing, K.Q.; supervision, K.Q. All authors have read and agreed to the published version of the manuscript.

Funding: This work was financially supported by Natural Science Foundation of China (grant number 41602095), the Key projects in National Science and Technology Pillar Program (grant number 2011BAB06B03), the Second Tibetan Plateau Scientific Expedition and Research Program (STEP) (grant number 2019QZKK0802, 2019QZKK0806), Key Research Program of the Institute of Geology and Geophysics, Chinese Academy of Sciences (grant number IGGCAS-201902), and National Geological Survey Project of Altay and Junggar (grant number DD20160006).

Acknowledgments: The authors are grateful to Qian Mao and Yueheng Yang for their help with the EMPA and LA-ICP-MS, respectively. Jinxiang Li, Junxing Zhao, Mingjian Cao, and Huaying Wu are thanked for their fruitful discussion and great suggestions that improved the quality of this manuscript. We also thank the reviewers for their valuable suggestions.

Conflicts of Interest: The authors declare no conflict of interest.

References

1. Jahns, R.H.; Burnham, C.W. Experimental studies of pegmatite genesis: I. A model for the derivation and crystallization of granitic pegmatites. *Econ. Geol.* **1969**, *64*, 843–864. [[CrossRef](#)]
2. London, D. *Pegmatites*; Special Publication 10; The Canadian Mineralogist: Quebec, QC, Canada, 2008; pp. 1–347.
3. Černý, P. Geochemical and petrogenetic features of mineralization in rare-element granite pegmatites in the light of current research. *Appl. Geochem.* **1992**, *7*, 393–416.
4. London, D. Granitic pegmatites: An assessment of current concepts and directions for the future. *Lithos* **2005**, *81*, 281–303. [[CrossRef](#)]
5. Canosa, F.; Matin-Izard, A.; Fuertes-Fuente, M. Evolved granitic systems as a source of rare-element deposits: The Ponte Segade case (Galicia, NW Spain). *Lithos* **2012**, *153*, 165–176. [[CrossRef](#)]
6. Černý, P. (Ed.) Petrogenesis of granitic pegmatites. In *Granitic Pegmatites in Science and Industry*; Short Course Handbook 8; Mineralogical Association of Canada: Quebec, QC, Canada, 1982; pp. 405–462.
7. Černý, P.; Meintzer, R.E.; Anderson, A.J. Extreme fractionation in rare-element granitic pegmatites: Selected examples of data and mechanisms. *Can. Mineral.* **1985**, *23*, 382–421.
8. Černý, P.; Ercit, T.S. The classification of granitic pegmatites revisited. *Can. Mineral.* **2005**, *43*, 2005–2026. [[CrossRef](#)]
9. Smeds, S.A. Trace elements in potassium-feldspar and muscovite as a guide in the prospecting for lithium- and tin-bearing pegmatites in Sweden. *J. Geochem. Explor.* **1992**, *42*, 351–369. [[CrossRef](#)]
10. Pichavant, M.; Villaros, A.; Deveaud, S.; Scaillet, B.; Lahlafi, M. Influence of redox state on mica crystallization in leucogranitic and pegmatitic liquids. *Can. Mineral.* **2016**, *54*, 559–581. [[CrossRef](#)]
11. Jolliff, B.L.; Papike, J.J.; Shearer, C.K. Fractionation trends in mica and tourmaline as indicators of pegmatite internal evolution: Bob Ingersoll pegmatite, Black Hills, South Dakota, USA. *Geochim. Cosmochim. Acta* **1987**, *51*, 519–534. [[CrossRef](#)]
12. Kile, D.E.; Foord, E.E. Micas from the Pikes Peak batholith and its cogenetic granitic pegmatites, Colorado: Optical properties, composition, and correlation with pegmatite evolution. *Can. Mineral.* **1998**, *36*, 463–482.
13. Roda, E.; Pesquera, A.; Gil-Crespo, P.P.; Torres-Ruiz, J.; de Parseval, P. Mineralogy and geochemistry of micas from the Pinilla de Fermoselle pegmatite (Zamora, Spain). *Eur. J. Mineral.* **2006**, *18*, 369–377. [[CrossRef](#)]
14. Roda, E.; Keller, P.; Pesquera, A.; Fontan, F. Micas of the muscovite-lepidolite series from Karibib pegmatites, Namibia. *Mineral. Mag.* **2007**, *71*, 41–62. [[CrossRef](#)]
15. Černý, P.; Burt, D.M. Paragenesis, crystallochemical characteristics, and geochemical evolution of micas in granite pegmatites. In *Micas*; Bailey, S.W., Ed.; Reviews in mineralogy 13; Mineralogical Society of America: Washington, DC, USA, 1984; pp. 257–297.
16. Henderson, C.M.B.; Martin, J.S.; Mason, R.A. Compositional relations in Li-micas from S.W. England and France: An ion- and electron-microprobe study. *Mineral. Mag.* **1989**, *53*, 427–449. [[CrossRef](#)]
17. Brigatti, M.F.; Lugli, C.; Poppi, L.; Foord, E.E.; Kile, D.E. Crystal chemical variations in Li- and Fe-rich micas from Pikes Peak batholith (central Colorado). *Am. Mineral.* **2000**, *85*, 1275–1286. [[CrossRef](#)]
18. Černý, P. Rare-element granitic pegmatites. Part I: Anatomy and internal evolution pegmatite deposits. *Geosci. Can.* **1991**, *18*, 49–67.
19. Černý, P. The Tanco rare-element pegmatite deposit, Manitoba: Regional context, internal anatomy, and global comparisons. In *Rare Element Geochemistry and Mineral Deposits*; Linnen, R.L., Samson, I.M., Eds.; Short Course Notes 17; Geological Association of Canada: Quebec, QC, Canada, 2004; pp. 184–231.
20. Foord, E.E.; Černý, P.; Jackson, L.L.; Sherman, D.M.; Eby, R.K. Mineralogical and geochemical evolution of micas from miarolitic pegmatites of the anorogenic Pikes Peak batholith, Colorado. *Mineral. Petrol.* **1995**, *55*, 1–26. [[CrossRef](#)]
21. Wise, M.A. Trace element chemistry of lithium—Rich micas from rare—Element granitic pegmatites. *Mineral. Petrol.* **1995**, *55*, 203–215. [[CrossRef](#)]
22. Pesquera, A.; Torres-Ruiz, J.; Gel-Crespo, P.; Velilla, N. Chemistry and genetic implications of tourmaline and Li-F-Cs micas from the Valdeflores area (Cáceres, Spain). *Am. Mineral.* **1999**, *84*, 55–69. [[CrossRef](#)]
23. Clarke, D.B.; Bogutyn, P.A. Oscillatory epitactic-growth zoning in biotite and muscovite from the Lake Lewis leucogranite, South Mountain batholith, Nova Scotia, Canada. *Can. Mineral.* **2003**, *41*, 1027–1047. [[CrossRef](#)]
24. Viana, R.R.; Jordt-Evangelista, H.; Stern, W.B. Geochemistry of muscovite from pegmatites of the Eastern Brazilian pegmatite province: A clue to petrogenesis and mineralization potential. *Eur. J. Mineral.* **2007**, *19*, 745–755. [[CrossRef](#)]
25. Vieira, R.R.; Roda-Robles, E.; Pesquera, A.; Lima, A. Chemical variation and significance of micas from the Fregeneda-Almendra pegmatitic field (Central-Iberian zone, Spain and Portugal). *Am. Mineral.* **2011**, *96*, 637–645. [[CrossRef](#)]
26. Li, J.; Huang, X.L.; He, P.L.; Li, W.X.; Yu, Y.; Chen, L.L. In situ analyses of micas in the Yashan granite, South China: Constraints on magmatic and hydrothermal evolutions of W and Ta-Nb bearing granites. *Ore Geol. Rev.* **2015**, *65*, 793–810. [[CrossRef](#)]
27. Villaros, A.; Pichavant, M. Mica-liquid trace elements partitioning and the granite-pegmatite connection: The St-Sylvestre complex (Western French Massif Central). *Chem. Geol.* **2019**, *528*, 119265. [[CrossRef](#)]
28. Zou, T.R.; Li, Q.C. *Rare and Rare Earth Metallic Deposits in Xinjiang, China*; Geological Publishing House: Beijing, China, 2006; pp. 1–284. (In Chinese with English Abstract)
29. Chen, F.W.; Li, H.Q.; Wang, D.H.; Cai, H.; Chen, W. New chronological evidence for Yanshanian diagenetic mineralization in China's Altay orogenic belt. *Chin. Sci. Bull.* **2000**, *45*, 108–114. [[CrossRef](#)]

30. Wang, D.H.; Chen, Y.C.; Zou, T.R.; Xu, Z.G.; Li, H.Q.; Chen, W.; Chen, F.W.; Tian, F. $^{40}\text{Ar}/^{39}\text{Ar}$ dating for the Azubai rare metal-gem deposit in Altay, Xinjiang—New evidence for Yanshanian mineralization of rare metals. *Geol. Rev.* **2000**, *46*, 307–311. (In Chinese with English Abstract)
31. Wang, D.H.; Chen, Y.C.; Xu, Z.G. Chronological study of Caledonian metamorphic pegmatite muscovite deposits in the Altay Mountains, northwestern China, and its significance. *Acta Geol. Sin.* **2001**, *75*, 419–425. (In Chinese with English Abstract)
32. Wang, D.H.; Chen, Y.C.; Xu, Z.G. $^{40}\text{Ar}/^{39}\text{Ar}$ isotope dating on muscovite from Indosinian rare metal deposits in Central Altay, Northwestern China. *Bull. Mineral. Petrol. Geochem.* **2003**, *22*, 14–17. (In Chinese with English Abstract)
33. Wang, D.H.; Zou, T.R.; Xu, Z.G.; Yu, J.J.; Fu, X.F. Advance in the study of using pegmatite deposits as the tracer of orogenic process. *Adv. Earth Sci.* **2004**, *19*, 614–620. (In Chinese with English Abstract)
34. Ren, B.Q.; Zhang, H.; Tang, Y.; Lv, Z.H. LA-ICP-MS U-Pb zircon geochronology of the Altai pegmatites and its geological significance. *Acta Mineral. Sin.* **2011**, *31*, 587–596. (In Chinese with English Abstract)
35. Lv, Z.H.; Zhang, H.; Tang, Y.; Guan, S.J. Petrogenesis and magmatic-hydrothermal evolution time limitation of Kelumute No.112 pegmatite in Altay, Northwestern China: Evidence from zircon U-Pb and Hf isotopes. *Lithos* **2012**, *154*, 374–391. [CrossRef]
36. Zhou, Q.F.; Qin, K.Z.; Tang, D.M.; Tian, Y.; Cao, M.J.; Wang, C.L. Formation age and evolution time span of the Koktokay No.3 pegmatite, Altai, NW China: Evidence from U-Pb zircon and $^{40}\text{Ar}/^{39}\text{Ar}$ muscovite ages. *Resour. Geol.* **2015**, *65*, 210–231. [CrossRef]
37. Lv, Z.H.; Zhang, H.; Tang, Y.; Liu, Y.L.; Zhang, X. Petrogenesis of syn-orogenic rare metal pegmatites in the Chinese Altai: Evidences from geology, mineralogy, zircon U-Pb age and Hf isotope. *Ore Geol. Rev.* **2018**, *95*, 161–181. [CrossRef]
38. Lv, Z.H.; Zhang, H.; Tang, Y. Anatexis origin of rare metal/earth pegmatites: Evidences from the Permian pegmatites in the Chinese Altai. *Lithos* **2021**, *380–381*, 105865. [CrossRef]
39. Zhang, A.C.; Wang, R.C.; Hu, H.; Zhang, H.; Zhu, J.C.; Chen, X.M. Chemical evolution of Nb-Ta oxides and zircon from the Koktokay No.3 granitic pegmatite, Altai, northwestern China. *Mineral. Mag.* **2004**, *68*, 739–756. [CrossRef]
40. Zhang, A.C.; Wang, R.C.; Jiang, S.Y.; Hu, H.; Zhang, H. Chemical and textural features of tourmaline from the spodumene-subtype Koktokay No. 3 pegmatite, Altai, northwestern China: A record of magmatic to hydrothermal evolution. *Can. Mineral.* **2008**, *46*, 41–58. [CrossRef]
41. Zhang, A.C.; Wang, R.C.; Li, Y.; Hu, H.; Lu, X.; Ji, J.; Zhang, H. Tourmalines from the Koktokay No. 3 pegmatite, Altai, NW China: Spectroscopic characterization and relationships with the pegmatite evolution. *Eur. J. Mineral.* **2008**, *20*, 143–154. [CrossRef]
42. Liu, C.Q.; Zhang, H. The lanthanide tetrad effect in apatite from the Altay No.3 pegmatite, Xingjiang, China: An intrinsic feature of the pegmatite magma. *Chem. Geol.* **2005**, *214*, 61–77. [CrossRef]
43. Wang, R.C.; Hu, H.; Zhang, A.C.; Fontan, F.; Parseval, P.D.; Jiang, S.Y. Cs-dominant polylythionite in the Koktokay #3 pegmatite, Altai, NW China: In situ micro-characterization and implication for the storage of radioactive cesium. *Contrib. Mineral. Petrol.* **2007**, *153*, 355–367.
44. Cao, M.J.; Zhou, Q.F.; Qin, K.Z.; Tang, D.M.; Evans, N.J. The tetrad effect and geochemistry of apatite from the Altay Koktokay No.3 pegmatite, Xinjiang, China: Implications for pegmatite petrogenesis. *Mineral. Petrol.* **2013**, *107*, 985–1005. [CrossRef]
45. Zhou, Q.F.; Qin, K.Z.; Tang, D.M.; Ding, J.G.; Guo, Z.L. Mineralogy and significance of micas and feldspars from the Koktokay No.3 pegmatitic rare-element deposit, Altai. *Acta Petrol. Sin.* **2013**, *29*, 3004–3022. (In Chinese with English Abstract)
46. Zhou, Q.F.; Qin, K.Z.; Tang, D.M.; Wang, C.L.; Tian, Y.; Sakyi, P.A. Mineralogy of the Koktokay No.3 pegmatite, Altai, NW China: Implications for evolution and melt-fluid processes of rare-metal pegmatites. *Eur. J. Mineral.* **2015**, *27*, 433–457. [CrossRef]
47. Xiao, X.C.; Tang, Y.Q.; Feng, Y.; Zhu, B.; Li, J.; Zhou, M. *Tectonics in Northern Xinjiang and Its Neighbouring Areas*; Geological Publishing: Beijing, China, 1992; pp. 1–169. (In Chinese with English Abstract)
48. Windley, B.F.; Kröner, A.; Guo, J.; Qu, G.; Li, Y.; Zhang, C. Neoproterozoic to Paleozoic geology of the Altai orogen, NW China: New zircon age data and tectonic evolution. *J. Geol.* **2002**, *110*, 719–737. [CrossRef]
49. Wang, T.; Hong, D.W.; Jahn, B.M.; Tong, Y.; Wang, Y.B.; Han, B.F.; Wang, X.X. Timing, petrogenesis and setting of Paleozoic syn-orogenic intrusions from the Altai Mountains, NW China: Implications for tectonic evolution of an accretionary orogen. *J. Geol.* **2006**, *114*, 735–751. [CrossRef]
50. Chen, B.; Jahn, B.M. Geochemical and isotopic studies of the sedimentary and granitic rocks of the Altai orogen of northwest China and their tectonic implications. *Geol. Mag.* **2002**, *139*, 1–13. [CrossRef]
51. Xiao, W.J.; Windley, B.F.; Yuan, C.; Sun, M.; Han, C.M.; Lin, S.F.; Chen, H.L.; Yan, Q.R.; Liu, D.Y.; Qin, K.Z.; et al. Paleozoic multiple subduction-accretion processes of the southern Altaids. *Am. J. Sci.* **2009**, *309*, 221–270. [CrossRef]
52. Tong, Y.; Wang, T.; Hong, D.W.; Dai, Y.J. TIMS U-Pb zircon ages of Fuyun post-orogenic linear granite plutons on the southern margin of Altay orogenic belt and their implications. *Acta Petrol. Mineral.* **2006**, *29*, 619–641. (In Chinese with English Abstract)
53. Yuan, C.; Sun, M.; Long, X.P.; Xia, X.P.; Xiao, W.J.; Li, X.H.; Lin, S.F.; Cai, K.D. Constraining the deposition time and tectonic background of the Habahe Group of the Altai. *Acta Petrol. Sin.* **2007**, *23*, 1635–1644. (In Chinese with English Abstract)
54. Cai, K.D.; Sun, M.; Yuan, C.; Zhao, G.C.; Xiao, W.J.; Long, X.P.; Wu, F.Y. Prolonged magmatism, juvenile nature and tectonic evolution of the Chinese Altai, NW China: Evidence from zircon U-Pb and Hf isotopic study of Paleozoic granitoids. *J. Asian Earth Sci.* **2011**, *42*, 949–968. [CrossRef]
55. Cai, K.D.; Sun, M.; Yuan, C.; Long, X.P.; Xiao, W.J. Geological framework and Paleozoic tectonic history of the Chinese Altai, NW China: A review. *Russ. Geol. Geophys.* **2011**, *52*, 1619–1633. [CrossRef]

56. Shen, X.M.; Zhang, H.X.; Wang, Q.; Wyman, D.A.; Yang, Y.H. Late Devonian-Early Permian A-type granites in the southern Altay Range, Northwest China: Petrogenesis and implications for tectonic setting of “A2-type” granites. *J. Asian Earth Sci.* **2011**, *42*, 986–1007. [[CrossRef](#)]
57. Xiao, W.J.; Windley, B.F.; Badarch, G.; Sun, S.; Li, J.L.; Qin, K.Z.; Wang, Z. Palaeozoic accretionary and convergent tectonics of the southern Altaids: Implications for the growth of central Asia. *J. Geol. Soc. Lond.* **2004**, *161*, 339–342. [[CrossRef](#)]
58. Sengör, A.M.C.; Natalín, B.A.; Burtman, V.S. Evolution of the Altaiid tectonic collage and Paleozoic crustal growth in Eurasia. *Nature* **1993**, *364*, 299–307. [[CrossRef](#)]
59. He, G.Q.; Li, M.S.; Liu, D.Q.; Zhou, N.H. *Palaeozoic Crustal Evolution and Mineralization in Xinjiang of China*; Xinjiang People’s Publishing House: Urumqi, China, 1994; pp. 1–437. (In Chinese)
60. Qin, K.Z. Metallogenesis in Relation to Central-Asia Style Orogeny of Northern Xinjiang. Post-Doctoral Research Report; Institute of Geology and Geophysics, Chinese Academy of Sciences: Beijing, China, 2000. (In Chinese with English Abstract)
61. Sun, M.; Long, X.P.; Cai, K.D.; Jiang, Y.D.; Wang, B.Y.; Yuan, C.; Zhao, G.C.; Xiao, W.J.; Wu, F.Y. Early Paleozoic ridge subduction in the Chinese Altai: Insight from the abrupt change in zircon Hf isotopic composition. *Sci. China* **2009**, *52*, 1345–1358. [[CrossRef](#)]
62. Li, J.Y.; Xiao, W.J.; Sun, G.H.; Gao, L.M. Neoproterozoic-Paleozoic tectonostratigraphy, magmatic activities and tectonic evolution of eastern Xinjiang, NW China. In *Tectonic Evolution and Metallogeny of the Chinese Altay and Tianshan*; Mao, J.W., Goldfarb, R.J., Seltmann, R., Wang, D.H., Xiao, W.J., Hart, C., Eds.; IAGOD Guidebook Series; CERCAMS/NHM 10: London, UK, 2003; pp. 31–74.
63. Wang, T.; Hong, D.W.; Tong, Y.; Han, B.F.; Shi, Y.R. Zircon U-Pb SHRIMP age and origin of post-orogenic Lamazhao granitic pluton from Altai orogen: Its implications for vertical continental growth. *Acta Petrol. Sin.* **2005**, *21*, 640–650. (In Chinese with English Abstract)
64. Li, P.F.; Yuan, C.; Sun, M.; Long, X.P.; Cai, K.D. Thermochronological constraints on the late Paleozoic tectonic evolution of the southern Chinese Altai. *J. Asian. Earth. Sci.* **2015**, *113*, 51–60. [[CrossRef](#)]
65. Broussolle, A.; Aguilar, C.; Sun, M.; Schulmann, K.; Štípká, P.; Jiang, Y.D.; Yu, Y.; Xiao, W.J.; Wang, S.; Miková, J. Polycyclic Paleozoic evolution of accretionary orogenic wedge in the southern Chinese Altai: Evidence from structural relationships and U-Pb geochronology. *Lithos* **2018**, *314*, 400424.
66. Xiao, W.J.; Windley, B.F.; Han, C.M.; Liu, W.; Wan, B.; Zhang, J.E.; Ao, S.J.; Zhang, Z.Y.; Song, D.F. Late Paleozoic to early Triassic multiple roll-back and orocinal bending of the Mongolia collage in Central Asia. *Earth Sci. Rev.* **2018**, *186*, 94–128. [[CrossRef](#)]
67. Tong, Y.; Wang, T.; Kovach, V.P.; Hong, D.W.; Han, B.F. Age and origin of Takeshiken postorogenic alkali-rich intrusive rocks in southern Altai, near the Mongolian border in China and its implications for continental growth. *Acta Petrol. Mineral.* **2006**, *22*, 1267–1278. (In Chinese with English Abstract)
68. Wang, T.; Tong, Y.; Jahn, B.M.; Zou, T.R.; Wang, Y.B.; Hong, D.W.; Han, B.F. SHRIMP U-Pb Zircon geochronology of the Altai No.3 Pegmatite, NW China, and its implications for the origin and tectonic setting of the pegmatite. *Ore Geol. Rev.* **2007**, *32*, 325–336. [[CrossRef](#)]
69. Wang, T.; Tong, Y.; Li, S.; Zhang, J.J.; Shi, X.J.; Li, J.Y.; Han, B.F.; Hong, D.W. Spatial and temporal variations of granitoids in the Altay orogen and their implications for tectonic setting and crustal growth: Perspectives from Chinese Altay. *Acta Petrol. Mineral.* **2010**, *29*, 595–618. (In Chinese with English Abstract)
70. Liu, F.; Zhang, Z.X.; Li, Q.; Zhang, C.; Li, C. New precise timing constraint for the Keketuohai No.3 pegmatite in Xinjiang, China and identification of its parental pluton. *Ore Geol. Rev.* **2014**, *56*, 209–219. [[CrossRef](#)]
71. Wang, C.L.; Qin, K.Z.; Tang, D.M.; Zhou, Q.F.; Shen, M.D.; Guo, Z.L.; Guo, X.J. Geochronology and Hf isotope of zircon for the Arskarto Be-Nb-Mo deposit in Altay and its geological implications. *Acta Petrol. Sin.* **2015**, *31*, 2337–2352. (In Chinese with English Abstract)
72. Zhou, Q.F.; Qin, K.Z.; Tang, D.M.; Wang, C.L.; Sakyi, P.A. LA-ICP-MS U-Pb zircon, columbite-tantalite and $^{40}\text{Ar}/^{39}\text{Ar}$ muscovite age constraints for the rare-element pegmatite dikes in the Altai orogenic belt, NW China. *Geol. Mag.* **2018**, *155*, 707–728. [[CrossRef](#)]
73. Xiao, W.J.; Windley, B.F.; Sun, S.; Li, J.L.; Huang, B.C.; Han, C.M.; Yuan, C.; Sun, M.; Chen, H.L. A tale of amalgamation of three Permo-Triassic collage systems in Central Asia: Oroclines, sutures, and terminal accretion. *Annu. Rev. Earth Planet. Sci.* **2015**, *43*, 477–507. [[CrossRef](#)]
74. Zheng, Y.; Chen, Y.J.; Cawood, P.A.; Wang, Y.J.; Chen, H.Y.; Zhang, L.; Li, D.F. Late Permian-Triassic metallogeny in the Chinese Altay Orogen: Constraints from mica $^{40}\text{Ar}/^{39}\text{Ar}$ dating on ore deposits. *Gondwana Res.* **2017**, *43*, 4–16. [[CrossRef](#)]
75. Liu, Y.L.; Zhang, H.; Tang, Y.; Zhang, X.; Lv, Z.H.; Zhao, J.Y. Petrogenesis and tectonic setting of the Middle Permian A-type granites in Altay, Northwestern China: Evidences from geochronological, geochemical, and Hf isotopic studies. *Geol. J.* **2018**, *53*, 527–546. [[CrossRef](#)]
76. Yuan, C.; Sun, M.; Xiao, W.J.; Li, X.H.; Chen, H.L.; Lin, S.F.; Xia, X.P.; Long, X.P. Accretionary orogenesis of the Chinese Altai: Insights from Paleozoic granitoids. *Chem. Geol.* **2007**, *242*, 22–339. [[CrossRef](#)]
77. Geng, X.X.; Chai, F.M.; Yang, F.Q.; Zuo, W.Z.; Guo, Z.L.; Liu, F.; Zhang, Z.X. Geochronology and genesis of the bimodal volcanic rocks in Dalawuzi from the southern margin of Altay, Xinjiang. *Acta Petrol. Sin.* **2010**, *26*, 2967–2980. (In Chinese with English Abstract)
78. Armstrong, J.T. CITZAF: Combined ZAF and phirho(Z) Electron Beam Correction Programs; California Institute of Technology: Pasadena, CA, USA, 1989.

79. Xie, L.W.; Zhang, Y.B.; Zhang, H.H.; Sun, J.F.; Wu, F.Y. In situ simultaneous determination of trace elements, U-Pb and Lu-Hf isotopes in zircon and baddeleyite. *Chin. Sci. Bull.* **2008**, *53*, 1565–1573. [[CrossRef](#)]
80. Griffin, W.L.; Powell, W.J.; Pearson, N.J.; O'Reilly, S.Y. GLITTER: Data reduction software for laser ablation ICP-MS. In *Laser Ablation-ICP-MS in the Earth Sciences*; Sylvester, P., Ed.; Short Course Series 40, Appendix 2; Mineralogical Association of Canada: Quebec, QC, Canada, 2008; pp. 204–207.
81. Tischendorf, G.; Gottesmann, B.; Förster, H.-J.; Trumbull, R.B. On Li-bearing micas: Estimating Li from electron microprobe analyses and an improved diagram for graphical representation. *Mineral. Mag.* **1997**, *61*, 809–834. [[CrossRef](#)]
82. Maneta, V.; Baker, D.R. The potential of lithium in alkali feldspars, quartz, and muscovite as a geochemical indicator in the exploration for lithium-rich granitic pegmatites: A case study from the spodumene-rich Moblan pegmatite, Quebec, Canada. *J. Geochem. Explor.* **2019**, *205*, 106336. [[CrossRef](#)]
83. Legros, H.; Marignac, C.; Mercadier, J.; Cuney, M.; Richard, A.; Wang, R.C.; Charles, N.; Lespinasse, M.Y. Detailed paragenesis and Li-mica compositions as recorders of the magmatic-hydrothermal evolution of the Maoping W-Sn deposit (Jiangxi, China). *Lithos* **2016**, *264*, 108–124. [[CrossRef](#)]
84. Li, P.; Li, J.K.; Chen, Z.Y.; Liu, X.; Huang, Z.B.; Zhou, F.C. Compositional evolution of the muscovite of Renli pegmatite-type rare-metal deposit, northeast Hunan, China: Implications for its petrogenesis and mineralization potential. *Ore Geol. Rev.* **2021**, *138*, 104830. [[CrossRef](#)]
85. London, D. A petrologic assessment of internal zonation in granitic pegmatites. *Lithos* **2014**, *184–187*, 74–104. [[CrossRef](#)]
86. London, D. Ore-forming processes within granitic pegmatites. *Ore Geol. Rev.* **2018**, *101*, 349–383. [[CrossRef](#)]
87. López-Moro, F.J.; Polonio, F.G.; Gonález, T.L.; Contreras, J.L.S.; Fernández, A.G.; Benito, M.C.M. Ta-Sn concentration by muscovite fractionation and degassing in a lens-like granite body: The case study of the Penouta rare-metal albite granite (NW Spain). *Ore Geol. Rev.* **2017**, *82*, 10–30. [[CrossRef](#)]
88. Breiter, K.; Hložková, M.; Korbelová, Z.; Galiová, M.V. Diversity of lithium mica compositions in mineralized granite-greisen system: Cnovec Li-Sn-W deposit, Erzgebirge. *Ore Geol. Rev.* **2019**, *106*, 12–27. [[CrossRef](#)]
89. Xie, L.; Wang, R.C.; Groat, L.A.; Zhu, J.C.; Huang, F.F.; Cempírek, J. A combined EMPA and LA-ICP-MS study of Li-bearing mica and Sn-Ti oxide minerals from the Qiguling topaz rhyolite (Qitianling District, China): The role of fluorine in origin of tin mineralization. *Ore Geol. Rev.* **2015**, *65*, 779–792. [[CrossRef](#)]
90. Guimarães, F.S.; de Oliveira, A.L.R.; Amorim, L.E.D.; Rios, F.J.; Lehmann, B.; Hernández, C.R.; Moraes, R. Lithium-mica composition as pathfinder and recorder of Grenvillian-age greisenization, Rondonia Tin Province, Brazil. *Geochemistry* **2021**, *81*, 125737. [[CrossRef](#)]
91. Shi, R.Z.; Zhao, J.X.; Evans, N.J.; Qin, K.Z.; Wang, F.Y.; Li, Z.Z.; Han, R.; Li, X.F. Temporal-spatial variations in Li-Fe mica compositions from the Weilasituo Sn-polymetallic deposit (NE China): Implications for deposit-scale fluid evolution. *Ore Geol. Rev.* **2021**, *134*, 104132. [[CrossRef](#)]
92. Van Lichtervelde, M.; Grégoire, M.; Linnen, R.L.; Béziat, D.; Salvi, S. Trace element geochemistry by laser ablation ICP-MS of micas associated with Ta mineralization in the Tanco pegmatite, Manitoba, Canada. *Contrib. Mineral. Petrol.* **2008**, *155*, 791–806. [[CrossRef](#)]
93. Oyarzábal, J.; Galliski, M.A.; Perino, E. Geochemistry of K-feldspar and Muscovite in rare-element pegmatites and granites from the Totoral pegmatite field, San Luis, Argentina. *Resour. Geol.* **2009**, *59*, 315–329. [[CrossRef](#)]
94. Černý, P. Rare-element granitic pegmatites. Part II: Regional to global environments and petrogenesis. *Geosci. Can.* **1991**, *18*, 68–81.
95. Hulbosch, N.; Hertogen, J.; Dewaele, S.; André, L.; Muchez, P. Alkali metal and rare earth element evolution of rock-forming minerals from the Gatumba area pegmatites (Rwanda): Quantitative assessment of crystal-melt fractionation in the regional zonation of pegmatite groups. *Geochim. Cosmochim. Acta* **2014**, *132*, 349–374. [[CrossRef](#)]
96. Černý, P.; Trueman, D.L.; Ziehlke, D.V.; Goad, B.E.; Paul, B.J. *The Cat Lake-Winnipeg River and Wekusku Lake Pegmatite Fields, Manitoba*; ER80-1; Department of Energy and Mines, Mineral Resources Division: Winnipeg, MB, Canada, 1981; 234p.
97. Lu, H.Z.; Wang, Z.G.; Li, Y.S. Magma-fluid transition and the genesis of pegmatite dike No.3, Altay, Xinjiang, Northwest China. *Chin. J. Geochem.* **1997**, *16*, 43–52.
98. Wang, R.C.; Hu, H.; Zhang, A.C.; Fontan, F.; Zhang, H.; Parseval, P.D. Occurrence and late re-equilibration of pollucite from the Koktokay No. 3 pegmatite, Altai, northwestern China. *Am. Mineral.* **2006**, *91*, 729–739. [[CrossRef](#)]
99. Wang, R.C.; Che, X.D.; Zhang, W.L.; Zhang, A.C.; Zhang, H. Geochemical evolution and late re-equilibration of Na-Cs-rich beryl from the Koktokay #3 pegmatite (Altai, NW China). *Eur. J. Mineral.* **2009**, *21*, 795–809.
100. Zhou, Q.F. The Geochronology, Mineralogy, Melt-Fluid Evolution and Metallogenesis of the Koktokay No.3 Pegmatitic Rare-Element Deposit, Altai, China. Ph.D. Thesis, Institute of Geology and Geophysics, Chinese Academy of Sciences, Beijing, China, 2013. (In Chinese with English Abstract)
101. Van Lichtervelde, M.; Salvi, S.; Béziat, D.; Linnen, R.L. Textural features and chemical evolution in tantalum oxides: Magmatic versus hydrothermal origins for Ta mineralization in the Tanco Lower Pegmatite, Manitoba, Canada. *Econ. Geol.* **2007**, *102*, 257–276. [[CrossRef](#)]
102. Thomas, R.; Davidson, P.; Beurlen, H. Tantalite-(Mn) from the Borborema Pegmatite Province, northeastern Brazil: Conditions of formation and melt and fluid-inclusion constraints on experimental studies. *Mineral. Depos.* **2011**, *46*, 749–759. [[CrossRef](#)]

103. Beurlen, H.; Thomas, R.; da Silva, M.R.R.; Müller, A.; Rhede, D.; Soares, D.R. Perspectives for Li- and Ta-mineralization in the Borborema pegmatite province, NE-Brazil: A review. *J. S. Am. Earth Sci.* **2014**, *56*, 110–127. [[CrossRef](#)]
104. Stepanov, A.; Mavrogenes, J.A.; Meffre, S.; Davidson, P. The key role of mica during igneous concentration of tantalum. *Contrib. Mineral. Petrol.* **2014**, *167*, 1009. [[CrossRef](#)]
105. Keppler, H. Influence of fluorine on the enrichment of high field strength trace elements in granitic rocks. *Contrib. Mineral. Petrol.* **1993**, *114*, 479–488. [[CrossRef](#)]
106. Linnen, R.L.; Keppler, H. Columbite solubility in granitic melts: Consequences for the enrichment and fractionation of Nb and Ta in the earth's crust. *Contrib. Mineral. Petrol.* **1997**, *128*, 213–227. [[CrossRef](#)]
107. Van Lichtervelde, M.; Holtz, F.; Melcher, F. The effect of disequilibrium crystallization on Nb-Ta fractionation in pegmatites: Constraints from crystallization experiments of tantalite-tapiolite. *Am. Mineral.* **2018**, *103*, 1401–1416. [[CrossRef](#)]
108. Pollard, P.; Pichavant, M.; Charoy, B. Contrasting evolution of fluorine-rich and boron-rich tin systems. *Miner. Dep.* **1987**, *22*, 315–321. [[CrossRef](#)]
109. Breiter, K.; Ackerman, L.; Ďurišová, J.; Svojtka, M.; Novák, M. Trace element composition of quartz from different types of pegmatites: A case study from the Moldanubian Zone of the Bohemian Massif (Czech Republic). *Mineral. Mag.* **2014**, *78*, 703–722. [[CrossRef](#)]
110. Icenhower, J.P.; London, D. An experimental study of element partitioning between biotite, muscovite and coexisting peraluminous granitic melt at 200 MPa (H_2O). *Am. Mineral.* **1995**, *80*, 1229–1251. [[CrossRef](#)]
111. Evensen, J.M.; London, D. Experimental silicate mineral/melt partition coefficients for beryllium and the crustal Be cycle from migmatite to pegmatite. *Geochim. Cosmochim. Acta* **2002**, *66*, 2239–2265. [[CrossRef](#)]
112. Stewart, D.B. Petrogenesis of lithium-rich pegmatites. *Am. Mineral.* **1978**, *63*, 970–980.
113. Pichavant, M.; Herrera, J.V.; Boulmier, S.; Briqueu, L.; Loron, J.L.; Juteau, M.; Marin, L.; Michard, A.; Sheppard, S.M.F.; Treuil, M.; et al. The Macusani glasses SE Peru: Evidence of chemical fractionation in peraluminous magmas. *Geochem. Soc. Sp. Pub.* **1987**, *1*, 359–374.
114. London, D. Geochemistry of alkali and alkaline earth elements in ore-forming granites, pegmatites and rhyolites. In *Rare Element Geochemistry and Mineral Deposits*; Linnen, R.L., Samson, I.M., Eds.; Geological Association of Canada Short Course Notes 17; Geological Association of Canada: Quebec, QC, Canada, 2005; pp. 17–43.
115. Linnen, R.L.; Van Lichtervelde, M.; Černý, P. Granitic pegmatites as sources of strategic metals. *Elements* **2012**, *8*, 275–280. [[CrossRef](#)]
116. Gallagher, M.J. Composition of some Rhodesian lithium-beryllium pegmatites. *Trans. Geol. Soc. S. Afr.* **1975**, *78*, 35–41.
117. Kretz, R.; Loop, J.; Hartree, R. Petrology and Li-Be-B geochemistry of muscovite-biotite granite and associated pegmatite near Yellowknife, Canada. *Contrib. Mineral. Petr.* **1989**, *102*, 174–190. [[CrossRef](#)]
118. Stilling, A. Bulk composition of the Tanco pegmatite at Bernic Lake, Manitoba, Canada. Master's Thesis, University of Manitoba, Winnipeg, MB, Canada, 1998.
119. Evensen, J.M.; London, D.; Wendlandt, R.F. Solubility and stability of beryl in granitic melts. *Am. Mineral.* **1999**, *84*, 733–745. [[CrossRef](#)]
120. London, D.; Evensen, J.M. Beryllium in silicic magmas and the origin of beryl-bearing pegmatites. In *Beryllium: Mineralogy, Petrology and Geochemistry*; Grew, E.S., Ed.; Mineralogical Society of America: Chantilly, VA, USA, 2002; p. 48.
121. Wedepohl, K.H. The composition of the continental crust. *Geochim. Cosmochim. Acta* **1995**, *59*, 1217–1232.
122. Rudnick, R.L.; Gao, S. Composition of the Continental Crust. *Treatise Geochem.* **2003**, *3*, 1–64.
123. Breaks, F.W.; Moore, J.M., Jr. The Ghost Lake batholith, Superior Province of Northwestern Ontario: A fertile, S-type peraluminous granite-rare element pegmatite system. *Can. Mineral.* **1992**, *30*, 835–875.
124. Kaeter, D.; Barros, R.; Menige, J.F.; Chew, D.M. The magmatic-hydrothermal transition in rare-element pegmatites from southeast Ireland: LA-ICP-MS chemical mapping of muscovite and columbite-tantalite. *Geochim. Cosmochim. Acta* **2018**, *240*, 98–130. [[CrossRef](#)]
125. Müller, A.; Romer, R.L.; Pedersen, R.-B. The Sveconorwegian pegmatite province—thousands of pegmatites without parental granites. *Can. Mineral.* **2017**, *55*, 283–315. [[CrossRef](#)]
126. Fan, J.J.; Tang, G.J.; Wei, G.J.; Wang, H.; Xu, Y.G.; Wang, Q.; Zhou, J.S.; Zhang, Z.Y.; Huang, T.Y.; Wang, Z.L. Lithium isotope fractionation during fluid exsolution: Implications for Li mineralization of the Bailongshan pegmatites in the West Kunlun, NW Tibet. *Lithos* **2020**, *352–353*, 105236. [[CrossRef](#)]
127. Maneta, V.; Baker, D.R.; Minarik, W. Evidence for lithium-aluminosilicate supersaturation of pegmatite-forming melts. *Contrib. Mineral. Petrol.* **2015**, *170*, 4. [[CrossRef](#)]
128. Maneta, V.; Baker, D.R. Exploring the effect of lithium on pegmatitic textures: An experimental study. *Am. Mineral.* **2014**, *99*, 1383–1403. [[CrossRef](#)]
129. Morgan, G.B.; London, D. Crystallization of the Little Three layered pegmatite-aplite dike, Ramona District, California. *Contrib. Mineral. Petrol.* **1999**, *136*, 310–330. [[CrossRef](#)]